Received: 13 August 2021 | Revised: 4 November 2021 | Accepted: 3 December 2021

DOI: 10.1096/fj.202101297R

THE FASEB JOURNAL

RESEARCH ARTICLE

Impact of metabolic disorders on the structural, functional, and immunological integrity of the blood-brain barrier: Therapeutic avenues

Madeeha H. Sheikh[1] | **Mariella Errede**[2] | **Antonio d'Amati**[2,3] | **Noorafza Q. Khan**[1] | **Silvia Fanti**[1] | **Rodrigo A. Loiola**[1,4] | **Simon McArthur**[5] | **Gareth S. D. Purvis**[1,6] | **Caroline E. O'Riordan**[1] | **Davide Ferorelli**[7] | **Alessandro Dell'Erba**[7] | **Julius Kieswich**[1] | **Chis Reutelingsperger**[8] | **Eugenio Maiorano**[3] | **Magdi Yaqoob**[1] | **Christoph Thiemermann**[1] | **Andrea Baragetti**[9,10] | **Alberico Luigi Catapano**[9,10] | **Giuseppe Danilo Norata**[9,10,11] | **Federica Marelli-Berg**[1] | **Daniela Virgintino**[2] | **Egle Solito**[1,12]

[1]William Harvey Research Institute, Barts and The London School of Medicine and Dentistry, Queen Mary University of London, London, UK

[2]Department of Basic Medical Sciences, Neurosciences and Sensory Organs, University of Bari School of Medicine, Bari, Italy

[3]Department of Emergency and Organ Transplantation, Section of Anatomic Pathology, University of Bari, Bari, Italy

[4]Laboratoire de la Barrière Hémato-Encéphalique, Faculty Jean Perrin, EA 2465, Université d'Artois, Arras, France

[5]Institute of Dentistry, Barts and The London School of Medicine and Dentistry, Queen Mary University of London, London, UK

[6]Sir William Dunn School of Pathology, University of Oxford, Oxford, UK

[7]Department of Interdisciplinary Medicine, Section of Legal Medicine, University of Bari, Bari, Italy

[8]Cardiovascular Research Institute, Maastricht University, Maastricht, The Netherlands

[9]Department of Pharmacological and Biomolecular Sciences, Milan University, Milan, Italy

[10]IRCCS Multimedica, Sesto San Giovanni, Italy

[11]S.I.S.A. Centre for the Study of Atherosclerosis-Bassini Hospital, Cinisello Balsamo, Italy

[12]Department of Medicina Molecolare e Biotecnologie Mediche, University of Naples "Federico II", Naples, Italy

Correspondence
Egle Solito, Centre for Translational Medicine and Therapeutics, William Harvey Research Institute, Barts and the London School of Medicine and Dentistry, Queen Mary University of London, Charterhouse Square, London EC1M 6BQ, UK.
Email: e.solito@qmul.ac.uk

Funding information
British Heart Foundation, Grant/Award Number: FS 16/60/32739;

Abstract

Mounting evidence has linked the metabolic disease to neurovascular disorders and cognitive decline. Using a murine model of a high-fat high-sugar diet mimicking obesity-induced type 2 diabetes mellitus (T2DM) in humans, we show that pro-inflammatory mediators and altered immune responses damage the blood-brain barrier (BBB) structure, triggering a proinflammatory metabolic phenotype. We find that disruption to tight junctions and basal lamina due to loss of control in the production of matrix metalloproteinases (MMPs) and their inhibitors (TIMPs) causes BBB impairment. Together the disruption to the structural and

Abbreviations: ANXA1, annexin A1; FPR, formyl peptide receptor.

Ministry of Education-CAPES, Brazil, Grant/Award Number: 7326/2014-09; Vini di Batasiolo S.p.A, Grant/Award Number: AL-RIC19ABARA_01; Fondazione Umberto Veronesi, Grant/Award Number: 2020-3318; Fondazione Cariplo, Grant/Award Number: 2016-0852, 2015-0524 and 2015-0564; Fondazione Telethon, Grant/Award Number: GGP19146; PRIN, Grant/Award Number: 2017K55HLC and 2017H5F943; H2020 REPROGRAM, Grant/Award Number: PHC-03-2015/667837-2; Ministero della Salute, Grant/Award Number: GR-2011-02346974; ERA NET, Grant/Award Number: ER-2017-2364981; FISM Fondazione Italianana Sclerosi Multipla, Grant/Award Number: 2014/R/21

functional integrity of the BBB results in enhanced transmigration of leukocytes across the BBB that could contribute to an initiation of a neuroinflammatory response through activation of microglia. Using a humanized in vitro model of the BBB and T2DM patient post-mortem brains, we show the translatable applicability of our results. We find a leaky BBB phenotype in T2DM patients can be attributed to a loss of junctional proteins through changes in inflammatory mediators and MMP/TIMP levels, resulting in increased leukocyte extravasation into the brain parenchyma. We further investigated therapeutic avenues to reduce and restore the BBB damage caused by HFHS-feeding. Pharmacological treatment with recombinant annexin A1 (hrANXA1) or reversion from a high-fat high-sugar diet to a control chow diet (dietary intervention), attenuated T2DM development, reduced inflammation, and restored BBB integrity in the animals. Given the rising incidence of diabetes worldwide, understanding metabolic-disease-associated brain microvessel damage is vital and the proposed therapeutic avenues could help alleviate the burden of these diseases.

KEYWORDS

basal lamina, blood-brain barrier, leukocytes migration, metabolic imbalance, MMPs, neuroinflammation

1 | BACKGROUND

Metabolic Syndrome (MetS)[1]—a cluster of at least three of the following traits: hyperglycemia, insulin resistance, abdominal obesity, high blood pressure, and dyslipidemia—have been linked with the development of neurovascular disease, including vascular dementia and neurodegenerative conditions such as Alzheimer's disease,[2] together termed the "metabolic-cognitive syndrome".[3] Low-grade chronic inflammation in MetS and subsequent development of Type 2 diabetes mellitus (T2DM) results in macrovascular and microvascular complications in peripheral vessels, but the impact on the brain microvasculature and blood-brain barrier (BBB) function remains elusive.

The BBB forms a specialized barrier between the interface of the peripheral and central systems, to maintain a homeostatic brain microenvironment. BBB dysfunction has been implicated in a growing number of CNS pathologies including multiple sclerosis,[4] Parkinson's disease,[5] and Alzheimer's disease.[2] Alteration of endothelial tight junctions (TJs) compromises the barrier function; impairing permeability, cell polarity, and transport systems and leading to secondary activation of astrocytes[6] and microglia.[7] Long-term BBB dysfunction can consequently cause neuronal dysfunction, injury, and degeneration.[8,9] Neuro-imaging in obese patients has revealed atrophy of the frontal lobes, hippocampus, and the thalamus while *post-mortem* studies of diabetic patients' brains have shown reduced grey and white matter, a hallmark of dementia.[10–12] In fact, rodents fed an unhealthy "western diet" have impaired memory retention and faster cognitive decline compared to chow-fed rodents.[13,14]

In this study, we have used a mouse model of high-fat high-sugar (HFHS) diet-induced T2DM to examine the structural, metabolic, and immunological changes at the BBB. We report that HFHF-feeding causes the dismantling of endothelial tight junctions and loss of vessel basal lamina (VBL) molecular components to impair BBB integrity. Moreover, metabolic overload is accompanied by a marked release of pro-inflammatory mediators and brain endothelial cell activation, which promote leukocyte migration into the brain parenchyma resulting in activation of microglia. We further report that therapeutic treatment with the pro-resolving protein hrANXA1 or *via* dietary changes can attenuate T2DM development with downstream effects on restoration of BBB structural, functional, and immunology integrity. In addition, we show the translatable applicability of our results using a humanized in vitro BBB model with T2DM patient serum and T2DM patient post-mortem brain studies. Our results find that T2DM patients have increased BBB leakage attributed to structural alterations at endothelial TJs and laminins that result in a marked increase in leukocyte presence within the brain parenchyma. These pathophysiological changes could be key in the development of the metabolic-cognitive syndrome.

2 | MATERIALS AND METHODS

2.1 | Animal experiments

This study was conducted in accordance to Arrive guidelines using 10-week-old male, wild-type C57BL/6 mice purchased from Charles River (UK). Mice were housed in temperature (25 ± 2°C) and humidity (55%) controlled rooms. Mice were fed either a normal chow-based diet (5053, LabDiet Ltd) or a high-fat high-sugar diet (58R3, HFHS, AIN-76A TestDiet) for 10 weeks as schematized in Figure S1.

2.2 | Measuring body weight and feeding behavior

All mice had free access to food and water, body weight was recorded weekly. The bodyweight of all animals was measured at the same time at the beginning of each week using the same balance for the whole experiment for the determination of body weight gain for measuring obesity.

Fresh food (150 g/cage) was also supplied at the beginning of each week and was regularly monitored through the week for color or consistency change. The diet from each cage was weighed before being changed to measure food (g/mouse/day) and calorie intake (kcal/mouse/day) using the following equations:

$$\text{Food intake} = \frac{\text{weight of diet at beginning of week} - \text{weight of diet at end of week}}{(\text{number of mice in cage} \times \text{number of days})}$$

2.3 | Treatment with hrANXA1 and dietary reversion

The pharmacological intervention was provided by treating 10-week-old male mice fed a HFHS-fed diet for 10 weeks with hrANXA1. The pharmacological intervention was provided from weeks 5 to 10, mice were treated with 33 μg/kg body weight hrANXA1 in 100 μl of 50 mM Hepes, 140 mM NaCl, given i.p/mouse 5 days/week. A dose of 33 μg/kg body weight was chosen based on previous studies.[15] The hrANXA1 was produced and purified as previously published.[16] Dietary intervention was provided by reverting mice fed a HFHS diet onto a standard chow diet. Ten-week-old male C57BL/6 mice were fed a HFHS diet for 10 weeks, after which mice were placed back on a chow diet for a further 5 weeks, the total dietary period for these mice was 15 weeks (Figure S1). All mice not treated with hrANXA1 were given a vehicle of 100 μl of 50 mM Hepes, 140 mM NaCl, pH 7.4, daily (5 times/week) i.p. chow-fed, HFHS-fed, and HFHS-fed + hrANXA1 mice were 20 weeks of age at cull. HFHS—chow reversion mice were 25 weeks of age at cull. Animal studies were conducted in tandem for each group $n = 55$ for chow, HFHS, and HFHS + hrANXA1 mice. With the exception of HFHS—chow reversion mice with an $n = 15$, however, chow, HFHS, and HFHS + hrANXA1 were also collected alongside the reversion diet mice.

All animal experimental procedures performed in this study were approved by the Animal Welfare Ethics Review Board (AWERB) of the Queen Mary University of London-UK. The study was performed under the Procedure Project License; PPL: 70/8350 issued by the home office. Animal welfare and performed protocols were conducted under the guidance of Operation of Animals (Scientific Procedures Act 1986) and the European Directive (2010/63/EU) on the protection of animals used for scientific purposes. All mice had access to food and water *ad libitum*. Assignment to diet and treatment was performed randomly and no blinding was performed.

2.4 | Metabolic analysis in mice

For oral glucose tolerance tests (OGTT) and insulin tolerance tests (ITT), mice were fasted for 6 h. Testing was carried out at weeks 8 or 9, respectively, or weeks 14 or 15 for HFHS—chow reversion mice. For measuring OGTT, mice were administered an oral bolus of glucose (2 g/kg in dH_2O) and for the ITT, mice were administered a dose of insulin (1 unit/kg in PBS, i.p.). Blood glucose was measured via tail vein puncture at time 0, followed by measuring at 15-min intervals for a total duration of 120 min, using a glucometer (Accu-Chek Compact System; Roche Diagnostics, Basel, Switzerland). Non-fasting blood glucose values were obtained using a glucometer immediately after cardiac exsanguination. Commercially available ELISA kits were used to measure serum levels of insulin (ThermoFisher Scientific), cholesterol (Abcam, Cambridge, UK), and triglycerides (Abcam, Cambridge, UK).

2.5 | Primary murine brain endothelial cell culture

Primary murine endothelial cells were isolated and cultured from brain capillary fragments as previously described.[15]

Briefly, the meninges, white matter, and choroid plexus were removed from extracted brains. The remaining grey matter underwent two stages of enzymatic digestion to degrade the extracellular matrix. First, using Collagenase II (Sigma) and DNase1 (Sigma), followed by density-dependent centrifugation in 20% BSA to separate the heavier capillary fragments from the lighter myelin, neurons, and astrocytic components. The second enzymatic digest of microvesseles used collagenase-dispase (Roche), after which microvessels were plated into Petri dishes coated in 0.2% rat tail collagen I (Corning). Cells were initially cultured in DMEM/F12 medium (ThermoFisher Scientific) supplemented with 15% FBS, 1ng/ml bFGF (Roche), 100 μg heparin (Sigma), 1× insulin-transferrin-selenium (Gibco), 4 μg/ml puromycin (Sigma) to obtain pure monoculture and 100 units/ml gentamycin (Gibco). From day 3, cells were kept in 10% FBS, and from day 4, the medium was prepared without puromycin. Cultures were maintained at 37°C in 5% CO_2 and passaged at 75% confluency.

2.6 | bEnd3 cell culture

Immortalized mouse brain-derived endothelial cells, bEnd.3[17] were cultured in DMEM 1g/L D-glucose culture medium (Gibco) supplemented with 10% FBS, 4 mM Glutamax (Gibco), 100 units/ml Gentamycin (Gibco), 50 μM β-Mercaptoethanol (Gibco), 1 mM Na-Pyruvate (Sigma-Aldrich), and 1× non-essential amino acids (Gibco). Cultures were maintained at 37°C in 5% CO_2 and passaged at 80%–90% confluency.

2.7 | hCMEC/D3 culture

Immortalized human cerebrovascular endothelial cell line/clone D3, hCMEC/D3,[18] were cultured in EBM-2 medium (Lonza) supplemented with 5% FBS and growth factors (hFGF, VEGF, R3-IGF-1, Ascorbic acid, hEGF, and gentamycin), as recommended by the manufacturer. Cultures were maintained at 37°C in 5% CO_2 and passaged at 80%–90% confluency.

2.8 | Evans blue dye assessment

In vivo permeability was assessed using Evans blue dye; 100 μl of 2% Evans blue dye (4 ml/kg) in 0.9% saline was injected intravenously into the tail vein.[15] After 1 h, mice were sacrificed. Brain hemispheres were collected, macerated, and homogenized; samples were analyzed spectrophotometrically, normalized to tissue weight, and expressed as a percentage of serum dye content.

2.9 | In vitro permeability assays

Primary brain endothelial cells, bEnd3 cells, or hCMEC/D3 were grown on Transwell polycarbonate filters (pore size, 0.4 μm; Sigma-Aldrich, UK) coated with calfskin collagen type I followed by bovine plasma fibronectin for seven days. bEnd3 cells were stimulated overnight with 10% mouse serum. hCMEC/D3 cells were stimulated overnight with 20% human serum. Paracellular permeability was assessed using 55–77-kDa FITC-dextran (3 mg/ml) as previously described.[19] Transendothelial electrical resistance (TEER) measurements were performed using the Epithelial Volt/Ohm (EVOM2) meter (World Precision Instruments, USA) cell-free insert resistance values were subtracted from values obtained in the presence of endothelial cells.

2.10 | Immunohistochemistry and confocal microscopy

The animals were anesthetized using a ketamine/xylazine cocktail, 90 mg and 4.5 mg/kg, respectively, by intraperitoneal injection and perfused with 2% paraformaldehyde (PFA) and 0.2% glutaraldehyde (GTA) in phosphate-buffered saline (PBS) solution given over 3 min. Whole brains were removed and post-fixed by immersion in the same fixative for 4 h at 4°C, then washed in PBS overnight (ON) at 4°C. Using a vibrating microtome (Leica Microsystems; Milton Keynes, UK), 30-μm sagittal sections, evenly spaced at 200 μm intervals, were cut from each hemisphere. The sections were stored in 0.02% PFA in PBS at 4°C as free-floating sections.

After permeabilization with 0.5% Triton X-100 in PBS, free-floating sections were incubated with single or combined primary antibodies (Table S2) at 4°C ON, appropriate fluorophore-conjugated secondary antibodies (Table S2) for 45 min at room temperature, and counterstained with TO-PRO3™ (diluted 1:10k in PBS; Invitrogen). The sections were collected on polylysine slides (Menzel-Glaser) and cover-slip with Vectashield® mounting medium (Vector Laboratories), and finally sealed with nail varnish. Negative controls were prepared by omitting the primary antibodies and mismatching the secondary antibodies. Sections were examined under a Leica TCS SP5 confocal laser scanning microscope (Leica Microsystems) using a sequential scan procedure. Confocal images were taken at 0.35 μm intervals through the x, y, and z axes of the section, with 40× and 63× oil immersion lenses.

Quantification of fluorescence intensity was performed at 63× magnification on the mouse ($n = 4$ for each experimental group) and human ($n = 6$; T2DM $n = 3$, controls $n = 3$) samples (35 sections/sample, 10 randomly selected

fields/section) using Cell F as image analysis software (Olympus Italia; Rozzano, Italy). Data plotting and statistical analysis were performed on GraphPad. Statistical differences were evaluated using the Student's *t*-test. The values were expressed as mean ± SD.

2.11 | Flow cytometry

All samples were acquired by flow cytometry using a LSR Fortessa (BD Biosciences) and analyzed with FlowJo version 10. All antibodies are Biolegend unless otherwise stated. Once all staining was conducted, cell pellets were re-suspended in 200 μl of $PBS^{+/+}$ ready for FACS analysis; tubes were stored at 4°C. Primary endothelial cells or lymphocytes were collected from experimental mice groups. For mouse sera samples, bEnd3 cells were stimulated overnight with 10% mouse serum. Cells were harvested, fixed in 2% PFA, and stained in FACS buffer. For cell surface staining of junctional proteins and adhesion molecules, the following antibodies were used: Occludin (ThermoFisher Scientific) with secondary antibody goat anti-mouse IgG-AF488 (Life Technologies), PECAM-1 AF488 (eBioscience), VE-Cadherin (Abcam) with secondary antibody goat anti-rabbit IgG-Cy3 (Abcam), ICAM-1-APC, VCAM-1-Pacific blue, and CD86-PE-Cy7. For mouse migration studies, the following antibodies were used: CD45-APC-Cy7, CD4-PE-Cy7. Intracellular staining for G/F actin required permeabilization using the Mouse Foxp3 buffer kit (BD Pharmingen). Actin ratio was determined by staining cells with DNase1 AF488 (ThermoFisher) which recognized G-actin and with Phalloidin-568 (ThermoFisher) which recognized F-actin, the ratio of the MFI determined the content of globular:fibrillar (G:F) actin ratio. For human samples, hCMEC/D3 cells were stimulated with HD or T2DM sera overnight, after which cells were harvested, fixed in 2% PFA, and stained using FACS buffer. In cell surface staining of junctional proteins and adhesion molecules, the following antibodies were used: Occludin (ThermoFisher Scientific) with secondary antibody goat anti-mouse IgG-AF405, PECAM-1 AF488 (eBioscience), and VE-Cadherin (Abcam) with secondary antibody goat anti-rabbit IgG-Cy3 (Abcam) and ICAM-1-APC (eBioscience).

2.12 | Transmigration assay

Polycarbonate transwell inserts (0.33 cm^2 surface area, pore size 5 μm; Sigma-Aldrich, UK) were coated with laminin (50 μg/ml, Sigma). Cells were seeded on the top compartment of the transwells and cultured for 72 h to allow confluent monolayers to form. On the day of the assay, 600 μl of complete medium was added to the lower compartment of the transwells. Isolated and expanded mouse lymphocytes were added to the top compartment (1×10^6 cells/transwells) and incubated for 4 h at 37°C in 5% CO_2. After 4 h, inserts were removed, and the entire volume of the lower compartment was collected to assess the migrated lymphocyte population. Lymphocytes adhered to monolayers were collected using 0.2% trypsin and served as the adhered population. Cells were stained and analyzed via flow cytometry.

2.13 | Zymography

Gelatin zymography was used for the detection of gelatinases MMP-1, MMP-2, and MMP-9 in brain microvessels. For each sample, 1 μg/lane was loaded for separation by non-reducing gel electrophoresis on a 7.5% acrylamide gel containing 1 mg/ml porcine skin gelatin (Sigma). Following electrophoresis, the gel was washed extensively with 50-mM Tris-HCL containing 2.5% Triton X-100, 5-mM $CaCl_2$, and 1-μM $ZnCl_2$ to remove SDS and incubated overnight in activation buffer (50-mM Tris-HCl containing 1% Triton X-100, 5-mM $CaCl_2$, and 1-μM $ZnCl_2$) at 37°C. After incubation, the gel was stained in Coomassie brilliant blue, MMPs were detected as clear bands against a blue background of the undegraded substrate. Images were acquired with a ChemidocMP imaging system (Bio-Rad) and analyzed using ImageJ (NIH, USA).

2.14 | Cytokine analysis

The Mouse Cytokine Array XL Kit or Proteome Profiler Human XL Cytokine Array Kit (R&D Systems, Minneapolis, USA) was used to analyze different cytokines, interleukins, chemokines, and acute-phase proteins in mouse brain microvessels or hCMEC/D3 cell lysates stimulated with 20% human serum. The Human MMP Antibody array (Abcam) was used to analyze MMPs and TIMPs in human serum or hCMEC/D3 cell lysates stimulated with 20% human serum. These kits are membrane-based sandwich immunoassays. Briefly, membranes were blocked with blocked buffer for 1 h followed by overnight incubation with samples at 2–8°C. Membranes were incubated with a detection antibody cocktail. Bound antibodies were detected using Streptavidin-HRP and Chemi Reagent mix. Image Studio™ Lite (LI-COR Biosciences, USA) software was used to analyze the data. Mouse serum TIMP-1 levels were measured using a Quantikine ELISA kit (R&D Systems). Human serum IL-6 and TNF-α were measured

using a multiplex Human Luminex Assay (R&D Systems) on the Luminex MAGPIX System (Luminex Corporation).

2.15 | Human studies

Blood samples were drawn from "healthy donors" (HD) and patients with T2DM of the population-based epidemiological "PLIC" (Progressione delle Lesioni Intimali Carotidee) study. Subjects gave their consent for participating in the study in accordance with the ethical approval (SEFAP/Pr0003F University of Milan 06/2/2001).[20] Subjects were followed at the Societa Italiana per lo studio dell'aterosclerosi (SISA), Centre for the Study of Atherosclerosis, Bassini Hospital, Milan, Italy. All patients and healthy volunteers gave written informed consent in adherence to the Declaration of Helsinki. Complete information about clinical history was available from outpatient's registries and/oral hospital archives. HD were selected based on the following inclusion criteria: No personal and familial history of T2DM, no renal damage [urinary creatinine/albumin ratio as an average of three different measurements was collected to check for this parameter (not shown)] and absence of hepatic steatosis (ultrasound-based as previously described).[21] T2DM diagnosis was defined following the international guidelines,[22] information about the disease duration as well as information about pharmacological treatments, and regimes were gathered from the outpatients' registries.

2.16 | Collection of patient characteristics

Blood samples were drawn after overnight fasting (10 h at least) from antecubital vein and collected in EDTA tubes (BD Vacuette®). Blood samples were then centrifuged at 3000 rpm for 12 min in order to separate plasma for glucose quantification. Determination of lipid profile, glucose levels, and liver enzymes was performed by an enzymatic method (hexokinase reaction) through automatic sample analyzer (RX Daytona, Randox Laboratories Ltd®, Crumlin, UK). Low-density lipoprotein cholesterol (LDL-C) was derived from the Friedewald formula.[23] Fatty liver index (FLI) was calculated from body mass index (BMI), waist circumference, gamma-glutamyltransferase (GGT), and triglyceride levels in the fasting condition.[24] Patient characteristics are reported in Table S1. Serum was isolated from whole blood in serum tubes (Vacutainer) and stored at −80°C. The serum used for all biological tests was decomplemented at 56°C for 20 min. Twenty percent serum was used to stimulate hCMEC/D3 cells overnight prior to conducting experiments.

2.17 | Human brain immunohistochemistry

For human brain post-mortem studies, the sampling and handling of the specimens were conformed to the ethical rules of the Department of Emergency and Organ Transplantation, Division of Pathology, University of Bari School of Medicine, Italy. The study was reviewed and approved by the Medical Ethics Committee of University Hospital of Bari, Italy in compliance with the principles stated in the Declaration of Helsinki. Human brain samples ($n = 6$, subdivided into two groups: 3 with a known diagnosis of T2DM and 3 controls without a medical history of relevant disorders) were taken during autopsy required for legal purposes. Once arrived at the mortuary, the cadaver was analyzed and the anatomic-chronological parameters were reported, with a particular interest in the temperature, and a diary was compiled with the temperature at which the cadaver stayed, to ensure a uniform, maximized antigenicity among the samples selected according to routine histopathological evaluation. During the autopsy, the skull was generally the first body district to be analyzed for autopsy. The whole brain was removed, and two samples were taken from frontal and parietal lobes, which included both the cerebral cortex and the subcortical white matter. The samples were immediately fixed in 2% PFA and 0.2% GTA in PBS for 48 h at 4° C, washed in PBS overnight at 4°C, and then submitted to the same histological procedure as described for mouse brains.

2.18 | Statistical analysis

All data are presented as mean ± standard error of mean (SEM) of n observations, where n denotes the number of animals studied and/or repeats. All statistical analysis was conducted using GraphPad Prism 8 (GraphPad Software, San Diego, California, USA). All data were tested for normality and analyzed by a Student's *t*-test or one-way ANOVA for multiple comparisons with post hoc analysis using Bonferroni's post hoc test. Results were considered significant at $p < .05$.

3 | RESULTS

A number of different animals models exist for the investigation of T2DM pathophysiology,[25] some of which have demonstrated leakage of the BBB under a diabetic state.[26] Here, we used our established mouse model of T2DM induced by feeding a HFHS diet for 10 weeks (Figure S1A)[16] to investigate the effect of metabolic overload on the

BBB. Diet-induced diabetic models work through causing obesity from imbalanced food intake and low energy expenditure.[25] Obesity is the single biggest risk factor for developing T2DM, through raising the levels of fatty acids, glucose, pro-inflammatory markers thereby altering hormones and metabolism due to the accumulation of fat deposition, leading to the development of insulin resistance.[27] The diet-induced models of diabetes are used to replicate the westernized lifestyle in humans, with increased intake of foods dense in fats and sugars along with a sedentary lifestyle. This was the rationale for using a diet that was high in both fats and sugars.

The rising incidence of obesity and T2DM and its associated macro- and micro-vascular complications requires the need for appropriate management of the disease that can be achieved through medical management or lifestyle changes. We, therefore, investigated the potential of either a pharmacological intervention or a dietary intervention to reduce, repair, and restore the damage incurred at the BBB by T2DM. The pharmacological intervention was provided by hrANXA1, whereby mice were fed a HFHS diet for 10 weeks along with hrANXA1 treatment (0.35 μg/kg body weight, i.p. 5 times/week) from week 5 of the diet for 6 weeks (HFHS + hrANXA1 treated mice, Figure S1B). We have previously shown that the anti-inflammatory molecule annexin A1 (ANXA1) is an important regulator of TJ tightness[15] and that prophylactic hrANXA1 treatment in the same diet-driven animal model of T2DM (HFHS-diet) prevented the development of peripheral microvascular complications (nephropathy and liver hepatosteatosis) through the restoration of insulin sensitivity.[16] Alternatively, the dietary intervention was provided by reverting mice that had been fed a HFHS diet for 10 weeks back on to a normal chow diet for a further 5 weeks (HFHS—chow reversion mice, Figure S1C).

Confirmation of metabolic disruption (obesity, hyperglycemia, dyslipidemia, and insulin resistance) in this mouse model was conducted by measurements of weight gain, fat mass (epididymal and inguinal), fasting and non-fasting blood glucose, OGTT, and ITT as well as serum insulin, cholesterol, and triglyceride levels (Figure 1). At the end of the 10-week feeding period, mice fed a HFHS diet presented with significantly increased body weight and fat mass when compared to chow-fed mice (Figure 1A–D). Both pharmacological and dietary interventions significantly reduced the overall weight gain and epididymal fat mass compared to HFHS-fed mice, which was more prominent in the HFHS—chow diet reversion group; no changes were seen in the inguinal fat mass (Figure 1A–D). Tests for hyperglycemia found raised non-fasted in HFHS-fed mice when compared to chow-fed mice (Figure 1E). Treatment with hrANXA1 and reversion diet significantly reduced the non-fasted blood glucose levels when compared to HFHS-fed diet mice, however, no changes were seen in the fasted blood glucose levels, with concentrations significantly higher across all HFHS-fed groups when compared to chow-fed mice (Figure 1E,H). Insulin resistance was confirmed using OGTT and ITT; measurement of the area under the curve (AUC) in both tests found HFHS-fed mice to have an impaired insulin response compared to chow-fed mice, although this was not significant for the ITT (Figure 1F,G,I,J). While HFHS-fed + hrANXA1-treated mice had improved glucose tolerance when compared to HFHS-fed mice, no changes were seen in HFHS-chow reversion mice (Figure 1F,G). While little changes were witnessed with the ITT, serum insulin levels were significantly elevated in HFHS-fed mice compared to chow-fed mice, that were reduced with both interventions, however, this was only statistically significant for HFHS-fed + hrANXA1 mice (Figure 1K). HFHS-fed mice were also found to have hyperlipidemia, as seen by elevated serum cholesterol and triglyceride levels compared to chow-fed mice that were significantly reduced with hrANXA1 treatment; HFHS—chow reversion mice showed trends toward improved lipid levels (Figure 1L,M).

In summary, it was seen that the HFHS-diet induced obesity and contributed to the development of MetS as noted by hyperglycemia, hyperinsulinemia, hypercholesterolemia, and hypertriglyceridemia. Generally, while both pharmacological and dietary interventions attenuate MetS development, treatment with hrANXA1 showed greater improvement across the majority of measures when compared to HFHS-fed mice, with a particular effect on improving serum levels and glucose tolerance. Furthermore, results showed the levels/concentrations in HFHS-fed + hrANXA1-treated mice were largely similar to those in chow-fed mice, with the exception of weight gain. The reduction of weight gain, in comparison, was the strongest indicator of improvement in the HFHS—chow reversion diet group suggest that diet has an important impact on obesity.

Following confirmation that HFHS-feeding causes metabolic disruption, we further determined that these mice exhibit brain microvascular disruption characterized by increased Evans blue dye leakage into the brain when compared to mice fed a standard chow diet (Figure 2A).

Having shown that both treatments with hrANXA1 and dietary reversion could improve HFHS-induced metabolic abnormalities, we investigated whether beneficial effects could be detected at the BBB. Indeed, both treatments improved BBB functionality as seen by a reduction in Evans blue dye leakage (Figure 2A). Further measurements of BBB integrity assessment were conducted in vitro using primary murine brain endothelial cells seeded on transwell inserts. Increased paracellular permeability to 55-77DA FITC-dextran tracer was seen in endothelial

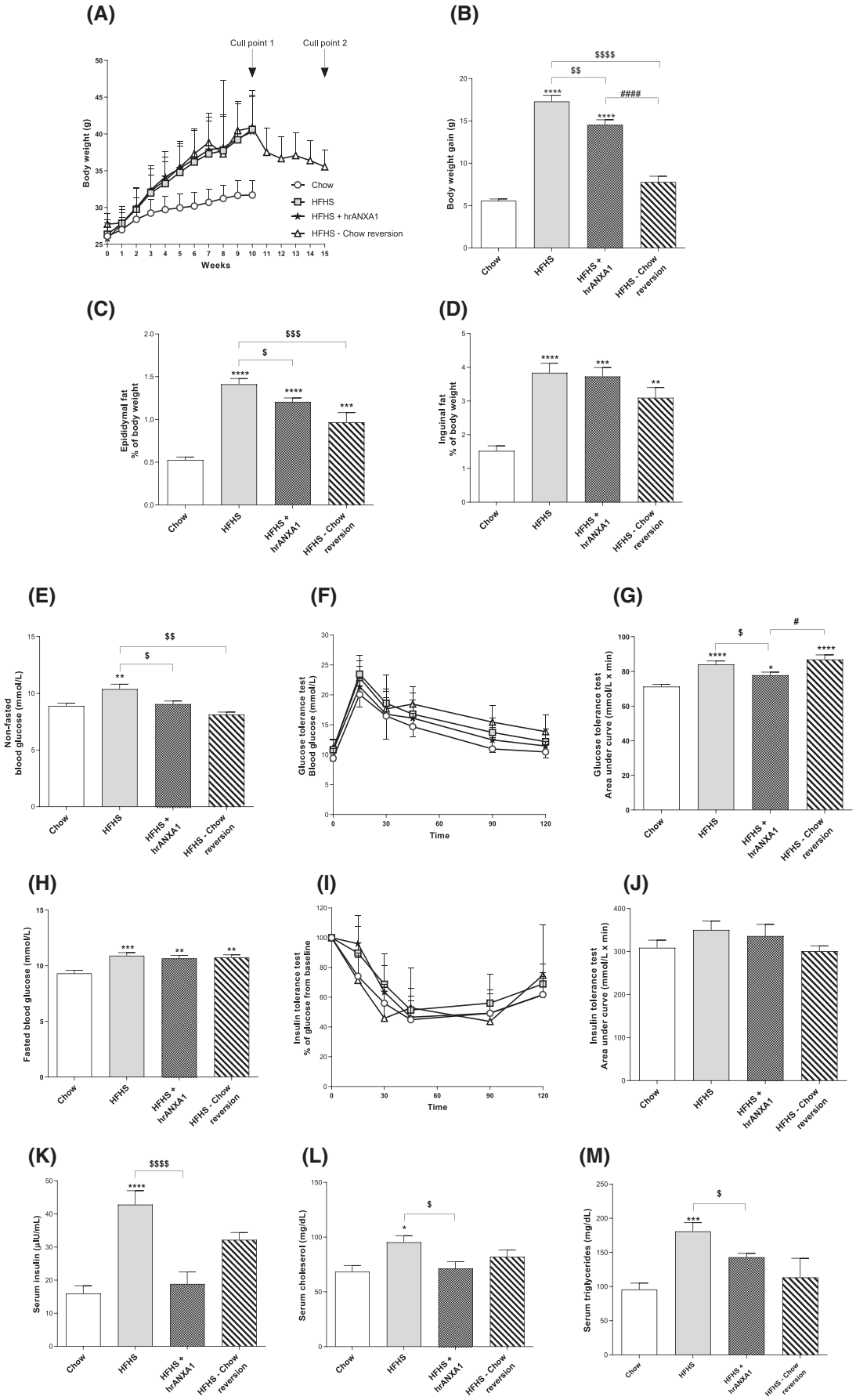
(A)
Cull point 1
Cull point 2
Body weight (g)
Weeks
Chow
HFHS
HFHS + hrANXA1
HFHS - Chow reversion
(B)
Body weight gain (g)
$$$$
$$
####
****
****
Chow
HFHS
HFHS + hrANXA1
HFHS - Chow reversion
(C)
Epididymal fat % of body weight
$$$
$
****
****
***
(D)
Inguinal fat % of body weight
****
***
**
(E)
Non-fasted blood glucose (mmol/L)
$$
$
**
(F)
Glucose tolerance test Blood glucose (mmol/L)
Time
(G)
Glucose tolerance test Area under curve (mmol/L x min)
$
#
****
*
****
(H)
Fasted blood glucose (mmol/L)
***
**
**
(I)
Insulin tolerance test % of glucose from baseline
Time
(J)
Insulin tolerance test Area under curve (mmol/L x min)
(K)
Serum insulin (µIU/mL)
$$$$
****
(L)
Serum cholesterol (mg/dL)
$
*
(M)
Serum triglycerides (mg/dL)
$
***

FIGURE 1 Treatment with hrANXA1 and a reversion diet attenuates the development of T2DM. C57BL/6 mice were fed either a standard diet (chow) or a high-fat high-sugar diet (HFHS) for 10 weeks. The pharmacological intervention was given by treating with human recombinant (hr) ANXA1 (1 μg/100 μl, i.p.) five times/week from weeks 5 to 10 ($n = 55$). Dietary intervention was provided by placing mice on a HFHS for 10 weeks, followed by a chow diet for 5 weeks (HFHS—chow reversion; $n = 15$). (A, B) Body weight gain of experimental mice groups over the 10- or 15-week diet period ($n = 15$–55/group). (C, D) Measurement of visceral fat (epididymal and inguinal) deposits as a percentage of overall body weight after 10 weeks of diet, as a measure of obesity ($n = 15$–55/group). (E) Basal non-fasted blood glucose was measured after 10 weeks of diet, one hour prior to harvest ($n = 15$–44/group). (H) Basal fasted blood glucose was measured after 6 h of fasting at week 8 ($n = 15$–39/group). (F–I) Oral glucose tolerance test (OGTT, 15–38/group) or Insulin tolerance test (ITT, $n = 6$–15/group) was assessed over 120 min, after 6 h of fasting at week 8 or week 9, respectively. (G, J) The area under the curve (AUC) of OGTT and ITT was calculated and used for statistical analysis. (K) Serum insulin ($n = 8$–27/group), (L) cholesterol ($n = 9$–23/group), and (M) triglycerides ($n = 9$–23/group) levels were measured in serum isolated from whole blood at harvest. Statistical analysis was performed by one-way ANOVA followed by a Bonferroni post hoc test. Data are expressed as mean ± SEM. $^{*}p < .05$, $^{**}p < .01$, $^{***}p < .001$, $^{****}p < .0001$ versus chow; $^{\$}p < .05$, $^{\$\$}p < .01$, $^{\$\$\$}p < .001$, $^{\$\$\$\$}p < .0001$ versus HFHS. $^{\#}p < .05$, $^{\#\#\#\#}p < .0001$ versus HFHS + hrANXA1

cells from HFHS-fed mice when compared to chow-fed mice (Figure 2B), concomitant with a decreased TEER (Figure 2C). Similar to in vivo BBB restoration, treatment with hrANXA1 in HFHS-fed mice or reversion to a chow diet restored BBB functionality in vitro through a reduction in paracellular permeability and improved TEER when compared to HFHS-fed mice (Figure 2B,C).

3.1 | Changes to tight junction and vessel basil lamina components

Structural BBB integrity depends on TJ effectiveness, therefore, we conducted immunohistochemistry on cortical mouse brain sections staining for TJ proteins claudin-5 and occludin alongside the VBL content of laminin and its subunits α2 and α4. Significant reductions in both claudin-5 and occludin staining patterns were observed in the cerebral cortex of HFHS-fed mice, together with a reduced pan-laminin reactivity, when compared to chow-fed mice (Figure 2D,E). In HFHS-fed mice, the linear and continuous staining pattern, typical of structurally preserved TJ strands, appeared thinner, interrupted for both claudin-5, and occludin (Figure 2D,E). Endothelial cells and perivascular astrocytes contribute to provide a highly restrictive and regulated interface at the BBB via the expression of VBL molecules of basement membranes (BMs).[28] Accordingly, we double immunostaining for pan-laminin/endothelial laminin α4 and laminin α4/astrocytic laminin α2. We observed a significant reduction of laminin molecules in HFHS-fed mice when compared to chow-fed mice (Figure 2F–H), with a relatively higher reduction of laminin α2 (Figure 2G). In chow-fed mice, double laminin α4/laminin α2 immunostaining clearly showed the different distribution of laminin subunits,[28,29] with laminin α2 primarily present in the astrocyte VBL layer (outer vessel surface) *vs* laminin α4 mainly restricted to the endothelial VBL layer (inner vessel surface), that is absent in HFHS-fed mice. Further double immunostaining with the astroglia marker GFAP and laminin α2 showed a clear co-localization of laminin α2 at the astrocyte $GFAP^{+}$ end-feet in chow-fed mice, suggestive of astrocytic end-feet embracing the microvessel structure to form an intact vessel, which is hardly distinguishable in HFHS-fed mice, where hypertrophic perivascular astrocytes showed a very low laminin α2 staining and detachment from the vessel structure (Figure 2H).

Disrupted TJ structure induced by HFHS-feeding was restored upon hrANXA1 treatment as seen by reinstated levels of occludin and claudin-5, similar in staining pattern to those observed in chow-fed mice (Figure 2D,E). Moreover, treatment with hrANXA1 in HFHS-fed mice showed restoration of laminin subunits α2 and α4, when compared to HFHS diet-fed mice (Figure 1F,G) that allowed for reinstatement of co-localized laminin α2 with $GFAP^{+}$ astrocyte perivascular end-feet to reform an intact-looking BBB (Figure 2H). In contrast, the reversion diet lacked any effect on BBB structure when compared to HFHS-fed mice, with no changes observed in claudin-5, occludin, endothelial laminin α4, or astrocytic laminin α2 staining, preventing reattachment of $GFAP^{+}$ astrocytic end-feet to the vessel structure (Figure 2D–H).

3.2 | The balance of MMPs and TIMPs

The role of matrix metalloproteases (MMPs) in TJ and VBL degradation is well established and could account for the observed loss of BBB integrity seen in HFHS-fed mice. Analysis of brain microvessels using a membrane-based sandwich immunoassay showed significantly increased levels of MMP-2 and MMP-9 in brain microvessels extracts of HFHS-fed mice when compared to chow-fed mice (Figure 3A). Confirmation of MMP proteolytic activity was conducted via zymography, where there was a significant increase in pro- and active MMP-2 and MMP-9 forms in HFHS-fed mice compared to chow-fed mice (Figure 3C–E).

Restoration of BBB integrity in the HFHS-fed + hrANXA1 mice could, therefore, be accounted by the

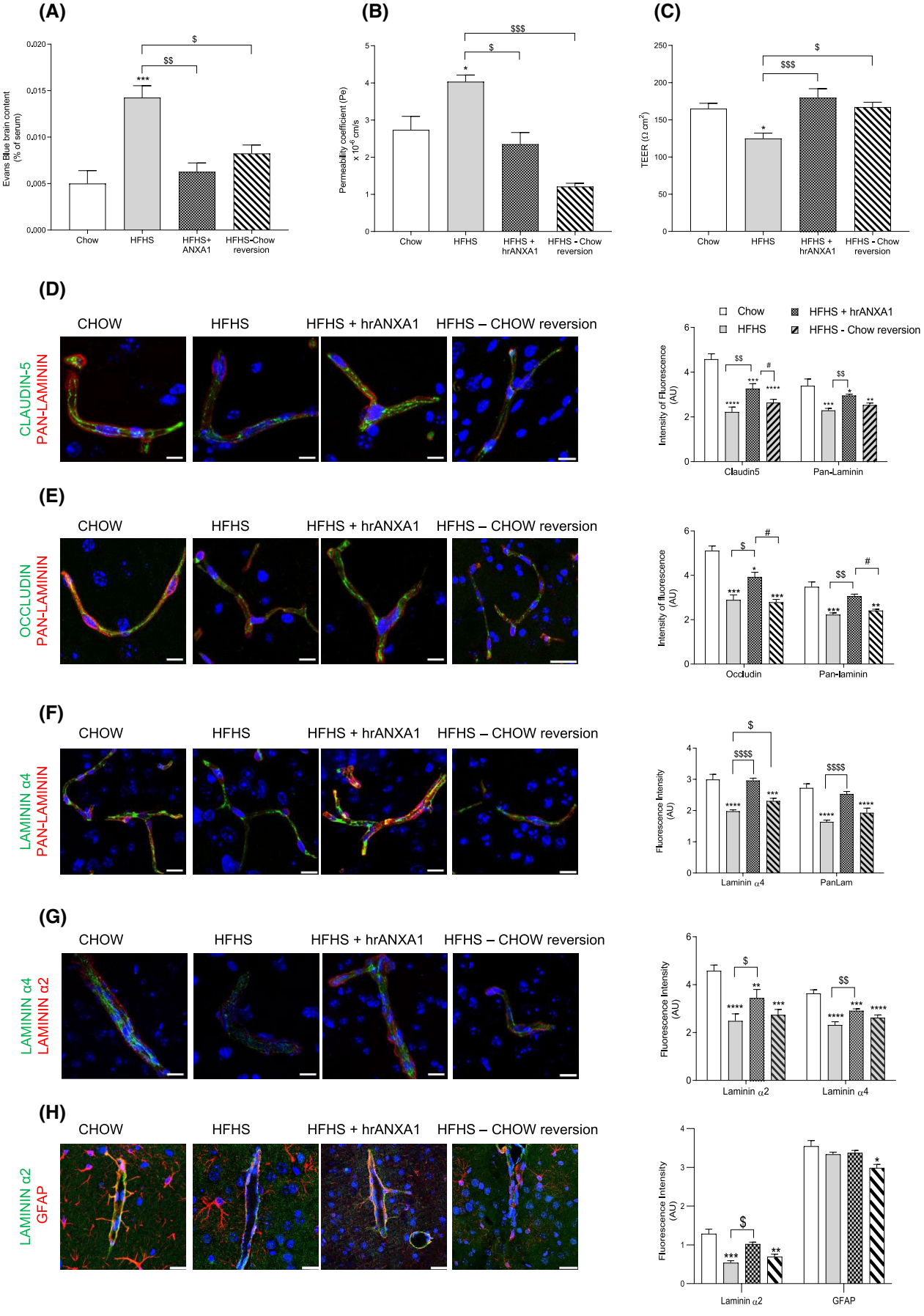
(A)
Evans Blue brain content (% of serum)
0.020
0.015
0.010
0.005
0.000
$
$$
***
Chow
HFHS
HFHS+ ANXA1
HFHS-Chow reversion
(B)
Permeability coefficient (Pe) x 10^-6 cm/s
5
4
3
2
1
0
$$$
$
*
Chow
HFHS
HFHS + hrANXA1
HFHS - Chow reversion
(C)
TEER (Ω cm^2)
250
200
150
100
50
0
$
$$$
*
Chow
HFHS
HFHS + hrANXA1
HFHS - Chow reversion
(D)
CHOW
HFHS
HFHS + hrANXA1
HFHS – CHOW reversion
CLAUDIN-5
PAN-LAMININ
Chow
HFHS
HFHS + hrANXA1
HFHS - Chow reversion
Intensity of Fluorescence (AU)
Claudin5
Pan-Laminin
(E)
CHOW
HFHS
HFHS + hrANXA1
HFHS – CHOW reversion
OCCLUDIN
PAN-LAMININ
Intensity of fluorescence (AU)
Occludin
Pan-laminin
(F)
CHOW
HFHS
HFHS + hrANXA1
HFHS – CHOW reversion
LAMININ α4
PAN-LAMININ
Fluorescence Intensity (AU)
Laminin α4
PanLam
(G)
CHOW
HFHS
HFHS + hrANXA1
HFHS – CHOW reversion
LAMININ α4
LAMININ α2
Fluorescence Intensity (AU)
Laminin α2
Laminin α4
(H)
CHOW
HFHS
HFHS + hrANXA1
HFHS – CHOW reversion
LAMININ α2
GFAP
Fluorescence Intensity (AU)
Laminin α2
GFAP

FIGURE 2 HFHS-feeding induces vascular leakage of the BBB due to loss of tight junction proteins and vessel basal lamina of endothelial cells and astrocytes, which is restored by pharmacological treatment with hrANXA1. C57BL/6 mice were fed either a standard diet (chow) or a high-fat high-sugar diet (HFHS) for 10 weeks. The pharmacological intervention was given by treating with human recombinant (hr) ANXA1 (1 μg/100 μl, i.p.) five times/week from weeks 5 to 10 (HFHS + hrANXA1). Dietary intervention was provided by placing mice on a HFHS for 10 weeks, followed by a chow diet for 5 weeks (HFHS—chow reversion). (A) In vivo assessment of BBB paracellular permeability via Evans blue dye extravasation ($n = 6$/group). (B) Measurement of paracellular permeability coefficients and (C) transendothelial electrical resistance (TEER) in primary mouse brain microvascular endothelial cells cultured from experimental mice groups using 70 kDA FITC-dextran and the Epithelial Volt/Ohm (EVOM2) Meter (World Precision Instruments, USA), respectively ($n = 10$ pooled/group, two technical replicates, performed as two-three independent experiments total $n = 20–30$). Confocal microscopy of cerebral cortical sections of mouse brains double immune-labeled with (D) claudin-5/pan-laminin, (E) occludin/pan-laminin, (F) endothelial laminin α4/pan-laminin, (G) astrocytic laminin α2/pan-laminin, and (H) astrocytic laminin α2/astrocytic marker glial fibrillary acidic protein (GFAP). Nuclei were labelled with TO-PRO3. Scale bar: 25 μm. Quantification of staining shown as mean fluorescence intensity (arbitrary units) of markers ($n = 4$ mice/group, 35 section/animal, 10 randomly selected fields/sections). Statistical analysis was performed by one-way ANOVA followed by a Bonferroni post hoc test. Data are expressed as mean ± SEM. $^{*}p < .05$, $^{**}p < .01$, $^{***}p < .001$, $^{****}p < .0001$ versus chow; $^{\$}p < .05$, $^{\$\$}p < .01$, $^{\$\$\$}p < .001$ versus HFHS; $^{\#}p < .05$, $^{\#\#\#}p < .001$ vs HFHS + hrANXA1

significantly reduced expression of MMP-9 (Figure 3A) and reduced activity of MMP-1, MMP-2, and MMP-9 (Figure 3B–E) in brain microvessels when compared to HFHS-fed mice, although statistical significance was not achieved when analyzing activity. Interestingly, despite the lack of BBB restoration, HFHS—chow reversion mice showed a significant reduction of MMP-1, MMP-2, and MMP-9 activity via the zymogram along with reduced expression of MMP-9 in the brain microvessels, when compared to HFHS-fed mice, levels of proteolytic activity in the reversion mice were similar to those seen in chow-fed mice (Figure 3A–E).

Inhibition of MMPs is mediated by the tissue inhibitor of metalloproteinases (TIMPs); through their binding to MMP domains.[30,31] Measurement of TIMP-1 in the sera of the mice revealed significantly reduced expression of TIMP-1 in HFHS-fed mice compared to chow-fed mice (Figure 3F). Both hrANXA1 treatment and dietary reversion increased serum levels of TIMP-1, albeit not to the levels seen in chow-fed mice and this effect only reached statistical significance in HFHS-fed + hrANXA1-treated mice (Figure 3F), suggesting that perhaps the balance of MMP/TIMPs is crucial in BBB remodeling.

On the contrary, MMP activity is regulated transcriptionally by reactive oxygen species (ROS), cytokines, growth factors, and hormones[32–34]; consequently, we measured such factors in the sera and brain microvessels of our mice (Figure 4). These measurements showed increased CXCL12, IL-1α, and sICAM-1 expression with decreased IL-13 expression in sera of HFHS-fed mice compared to chow-fed mice (Figure 4A). Within the serum, treatment of HFHS-fed mice with hrANXA1 significantly reduced the levels of the majority of pro-inflammatory species investigated, including CXCL1, CXCL12, IL-1α, IL-16, s-ICAM-1, and TNF-α (Figures 4A and S2), although there was not a corresponding increase in anti-inflammatory markers such as IL-13.

Analysis of isolated brain microvessel also revealed a disturbance in the levels of cytokines, chemokines, and interleukins in HFHS-fed mice compared to chow-fed mice (Figures 4B–E and S2), indicative of a raised inflammatory state at the BBB. Microvessels from HFHS-fed + hrANXA1-treated animals showed a general suppression of most inflammatory factors, a slight increase in both neutrophil/monocyte- and B/T-lymphocyte- directed chemokines but more limited effects on pro- and anti-inflammatory cytokines (Figures 4B–E and S2). HFHS—chow reversion diet mice showed greater changes with suppression in inflammatory factors, pro- and anti-inflammatory cytokines, and neutrophil/monocyte-directed chemokines, albeit with only minor effects on B/T-lymphocyte directed chemokines (Figures 4B–E and S2). In summary, both pharmacological and dietary intervention had generalized anti-inflammatory effects, with diet reversion being the more potent of the two, perhaps accounting for the greater reduction in MMP activity seen with dietary reversion vs hrANXA1 treatment. MMP-2 and MMP-9 promoter regions contain transcription factor binding sites such as AP-1 and NF-kB[34] that are regulated by the activation of signaling pathways such as ERK 1/2, JNK, and p38 MAP kinases (MAPK).[35–38] To investigate whether enhanced inflammatory mediator presence in HFHS-fed mice could thus contribute to the observed MMP upregulation/activation at the brain microvessels, western blot analysis of immortalized bEnd3 cells stimulated with sera from mice fed a chow or HFHS diet was conducted. Results identified Akt, SAPK/JNK, and p38 MAPK as potential signal transduction pathways responsible for MMP-mediated endothelial TJ dismantling and laminin degradation (Figure S3A–C), with all three proteins showing enhanced phosphorylation in brain endothelial cells, stimulated with sera from HFHS-fed mice.

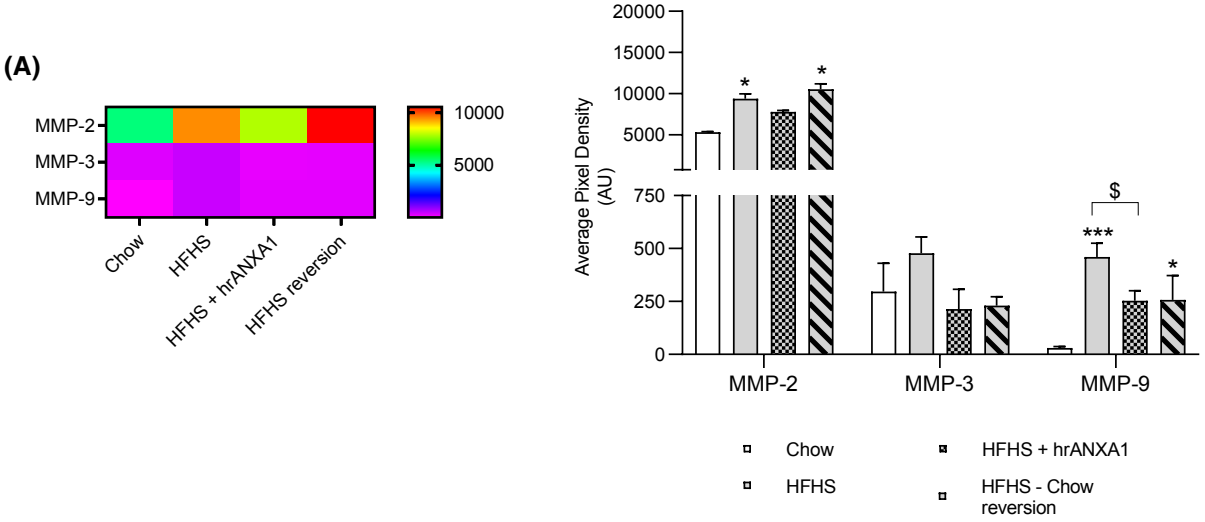
(A)
MMP-2
MMP-3
MMP-9
10000
5000
Chow
HFHS
HFHS + hrANXA1
HFHS reversion
Average Pixel Density (AU)
20000
15000
10000
5000
750
500
250
0
*
*
$
***
*
MMP-2
MMP-3
MMP-9
Chow
HFHS
HFHS + hrANXA1
HFHS - Chow reversion

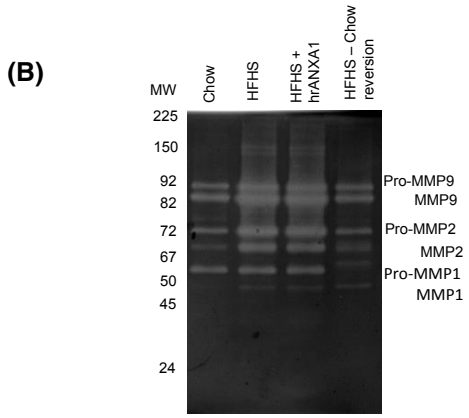
(B)
MW
Chow
HFHS
HFHS + hrANXA1
HFHS – Chow reversion
225
150
92
82
72
67
50
45
24
Pro-MMP9
MMP9
Pro-MMP2
MMP2
Pro-MMP1
MMP1

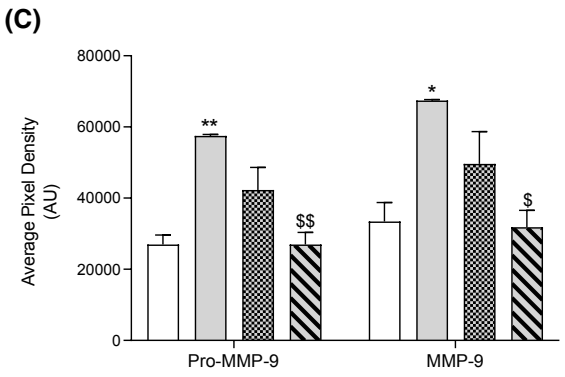
(C)
Average Pixel Density (AU)
80000
60000
40000
20000
0
**
$$
*
$
Pro-MMP-9
MMP-9

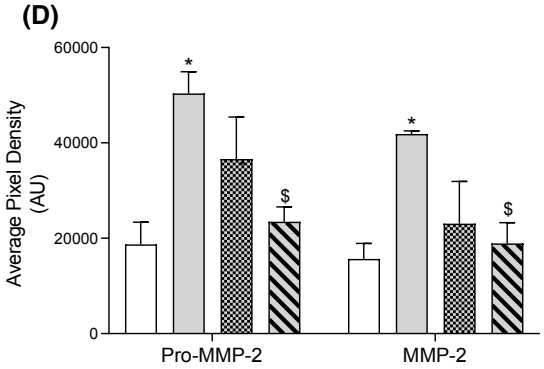
(D)
Average Pixel Density (AU)
60000
40000
20000
0
*
$
*
$
Pro-MMP-2
MMP-2

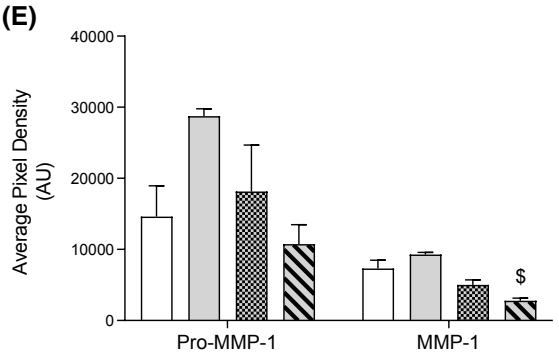
(E)
Average Pixel Density (AU)
40000
30000
20000
10000
0
$
Pro-MMP-1
MMP-1

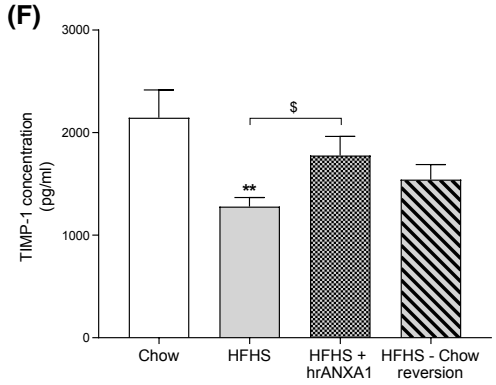
(F)
TIMP-1 concentration (pg/ml)
3000
2000
1000
0
$
**
Chow
HFHS
HFHS + hrANXA1
HFHS - Chow reversion

FIGURE 3 Increased MMP activity and loss of MMP/TIMP balance in HFHS-fed mice are responsible for the loss of the BBB structure. hrANXA1 treatment and dietary intervention reduce MMP activity at the BBB. (A) Expression of MMP-2, MMP-3, and MMP-9 was analyzed in brain microvessel extracts of chow-fed, HFHS-fed, HFHS-fed + hrANXA1-treated and HFHS—chow reversion diet mice using a Mouse Proteome Profiler, expressed as arbitrary units. ($n = 10$ pooled/group, two technical replicates per experiment, performed in duplicate total $n = 20$/group). (B) Proteolytic activity of MMP-2 and MMP-9 in brain microvessel extracts was determined via zymography, and (C–E) quantified panel ($n = 5$ pooled/group, representative gel of three independent experiments total $n = 15$), and (F) serum levels of tissue inhibitor of metalloproteinases (TIMP-1) were measured using a quantikine ELISA kit ($n = 11$/group). Statistical analysis was performed by one-way ANOVA followed by a Bonferroni post hoc test. Data are expressed as mean ± SEM. $^{*}p < .05$, $^{**}p < .01$, $^{***}p < .001$. $^{****}p < .0001$ versus chow; $^{\$}p < .05$, $^{\$\$}p < .01$, $^{\$\$\$}p < .001$ versus HFHS; $^{\#}p < .05$, $^{\#\#}p < .01$, $^{\#\#\#}p < .001$ vs HFHS + hrANXA1

Further ex vivo histological analysis in mice brains, showed a threefold increase in inflammation-associated inducible nitric oxide synthase (iNOS) staining, primarily localized on the cortex microvessels, in HFHS-fed mice when compared to chow-fed mice (Figure 4F). Both pharmacological and dietary intervention reduced iNOS staining, indicating a role for circulating inflammatory mediators in contributing to the damage of the BBB.

The impact of enhanced inflammatory mediator presence (locally and in the blood circulation) and the higher expression of iNOS was investigated at the microglia level. Microglia cells sense brain parenchyma alterations and are activated by circulating pro-inflammatory factors and hormones; and, therefore, a leaky BBB may also affect their functionality.[39] Confocal microscopy of brain sections stained for Iba1, a microglia activation marker, showed activated microglia of the HFHS-fed mice when compared to chow-fed mice (Figure 4G), suggesting inflammation and/or injury occurring within the brain. HFHS-fed + hrANXA1 mice and HFHS—chow reversion diet mice both presented with significantly reduced Iba1 immunostaining compared to HFHS-fed mice; notably, HFHS—chow reversion mice still had constitutively activated Iba1^{+} microglia in comparison to chow-fed and HFHS-fed + hrANXA1-treated mice (Figure 4G).

3.3 | A leaky BBB phenotype correlated with increased transmigration of leukocytes into the brain parenchyma

Both in vitro and in vivo studies have linked hyperglycemia and hyperlipidemia in T2DM to endothelial activation with enhanced expression of activation markers such as ICAM-1.[40] We, therefore, examined whether a HFHS-diet exerted similar effects on the BBB and its interaction with immune cells. We first analyzed the expression of ICAM-1 and P-selectin in the cerebral cortex by confocal microscopy and immunofluorescence quantification. Major differences in expression of ICAM-1 (Figure 5A) and P-selectin (Figure 5B) were observable with chow-fed mice showing a very low constitutive endothelial expression of both the adhesion molecules, whereas expression was significantly increased in HFHS-fed mice (Figure 5A,B). Treatment with hrANXA1 in HFHS-fed mice and HFHS—chow reversion diet mice showed reduced ICAM-1 and P-selectin expression, although this was only significant in HFHS-fed + hrANXA1 mice and the expression remained significantly higher than in chow-fed mice (Figure 5A,B). Further analysis of primary-isolated brain microvessels endothelial cells from chow- and HFHS-fed mice confirmed upregulated expression of adhesion molecules ICAM-1, P-selection, and VCAM-1 in HFHS-fed mice (Figure 5C); no changes were observed in the expression of E-selectin and co-stimulatory molecule CD40 (Figure 5C). Both interventions significantly reduced ICAM-1 and VCAM-1 expression, when compared to HFHS-fed mice (Figure 4C); CD40, E-selectin, and P-selectin reduction in HFHS—chow reversion diet-fed mice cerebral microvessels were not significant when compared to HFHS-fed mice (Figure 5C).

Next, we analyzed whether loss of BBB structure (TJ and astrocytic end-feet), increased inflammatory cytokine, and enhanced adhesion molecule expression correlated with increased immune cell extravasation into the brain parenchyma, as is known to occur in the peripheral system in T2DM. Cerebral cortex immunostaining for CD45 and pan-laminin demonstrated that CD45^{+} leukocytes, which were virtually absent in chow-fed mice were instead detected and relatively numerous and associated with cortex microvessels of HFHS-fed mice. In the latter, CD45^{+} cells were detectable both within the capillary lumen as well as enclosed in the two layers of the VBL or were seen in the act of moving toward the surrounding parenchyma (Figure 5D). Treatment with hrANXA1 resulted in no or rare CD45^{+} cells infiltration of the brain parenchyma (Figure 5D). However, diet reversion did not show any alterations in the CD45^{+} infiltration when compared to HFHS-fed mice, with confocal imaging showing entrapped CD45^{+} cells within the VBL layers.

Further assessments were performed using in vitro adhesion/migration experiments whereby isolated lymphocytes from deep cervical lymph nodes were activated and expanded for 4 days using CD3 and CD28, after which

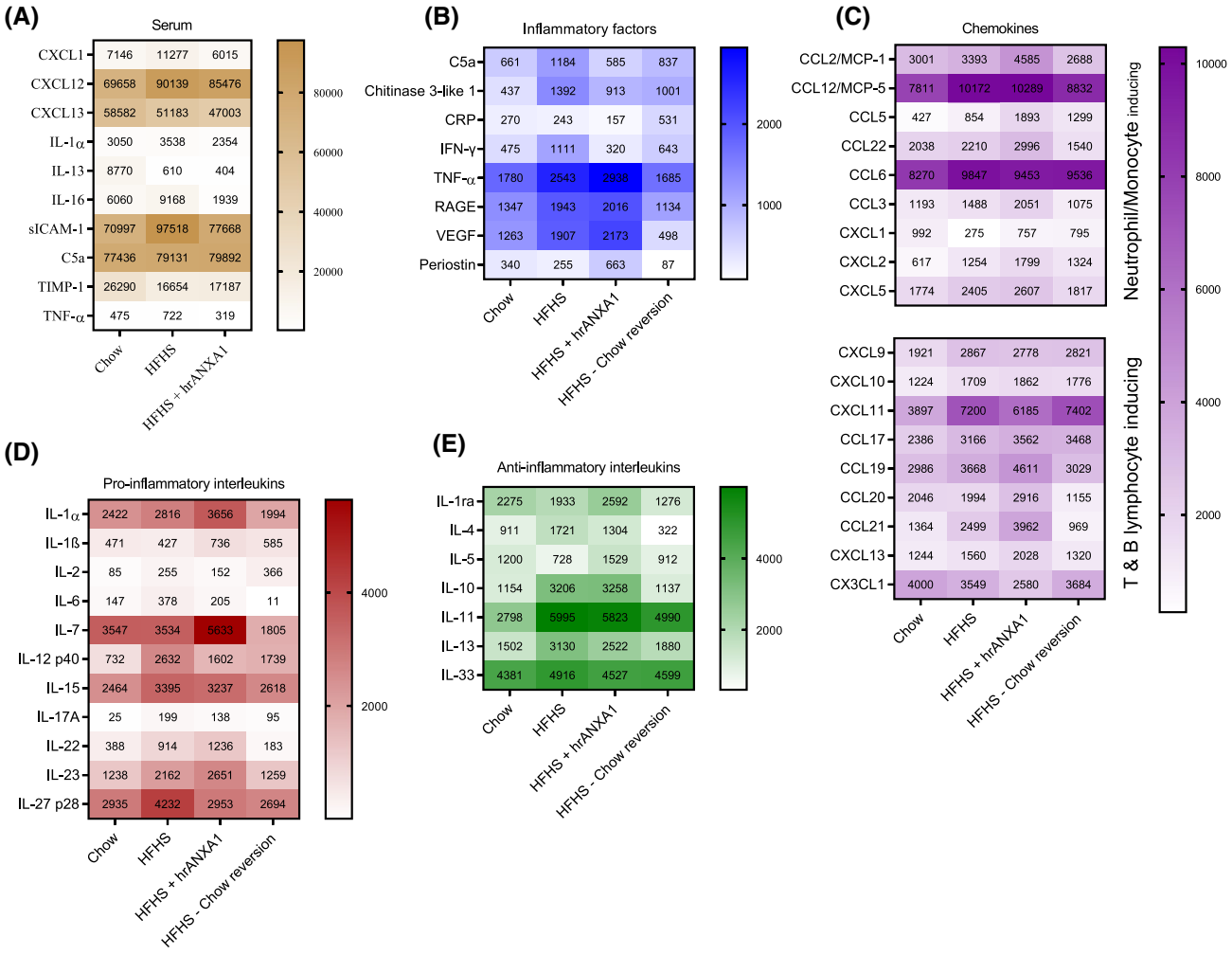
(A)
Serum
CXCL1 7146 11277 6015
CXCL12 69658 90139 85476
CXCL13 58582 51183 47003
IL-1α 3050 3538 2354
IL-13 8770 610 404
IL-16 6060 9168 1939
sICAM-1 70997 97518 77668
C5a 77436 79131 79892
TIMP-1 26290 16654 17187
TNF-α 475 722 319
80000
60000
40000
20000
Chow
HFHS
HFHS + hrANXA1
(B)
Inflammatory factors
C5a 661 1184 585 837
Chitinase 3-like 1 437 1392 913 1001
CRP 270 243 157 531
IFN-γ 475 1111 320 643
TNF-α 1780 2543 2938 1685
RAGE 1347 1943 2016 1134
VEGF 1263 1907 2173 498
Periostin 340 255 663 87
2000
1000
Chow
HFHS
HFHS + hrANXA1
HFHS - Chow reversion
(C)
Chemokines
CCL2/MCP-1 3001 3393 4585 2688
CCL12/MCP-5 7811 10172 10289 8832
CCL5 427 854 1893 1299
CCL22 2038 2210 2996 1540
CCL6 8270 9847 9453 9536
CCL3 1193 1488 2051 1075
CXCL1 992 275 757 795
CXCL2 617 1254 1799 1324
CXCL5 1774 2405 2607 1817
Neutrophil/Monocyte inducing
CXCL9 1921 2867 2778 2821
CXCL10 1224 1709 1862 1776
CXCL11 3897 7200 6185 7402
CCL17 2386 3166 3562 3468
CCL19 2986 3668 4611 3029
CCL20 2046 1994 2916 1155
CCL21 1364 2499 3962 969
CXCL13 1244 1560 2028 1320
CX3CL1 4000 3549 2580 3684
T & B lymphocyte inducing
10000
8000
6000
4000
2000
Chow
HFHS
HFHS + hrANXA1
HFHS - Chow reversion
(D)
Pro-inflammatory interleukins
IL-1α 2422 2816 3656 1994
IL-1ß 471 427 736 585
IL-2 85 255 152 366
IL-6 147 378 205 11
IL-7 3547 3534 5633 1805
IL-12 p40 732 2632 1602 1739
IL-15 2464 3395 3237 2618
IL-17A 25 199 138 95
IL-22 388 914 1236 183
IL-23 1238 2162 2651 1259
IL-27 p28 2935 4232 2953 2694
4000
2000
Chow
HFHS
HFHS + hrANXA1
HFHS - Chow reversion
(E)
Anti-inflammatory interleukins
IL-1ra 2275 1933 2592 1276
IL-4 911 1721 1304 322
IL-5 1200 728 1529 912
IL-10 1154 3206 3258 1137
IL-11 2798 5995 5823 4990
IL-13 1502 3130 2522 1880
IL-33 4381 4916 4527 4599
4000
2000
Chow
HFHS
HFHS + hrANXA1
HFHS - Chow reversion

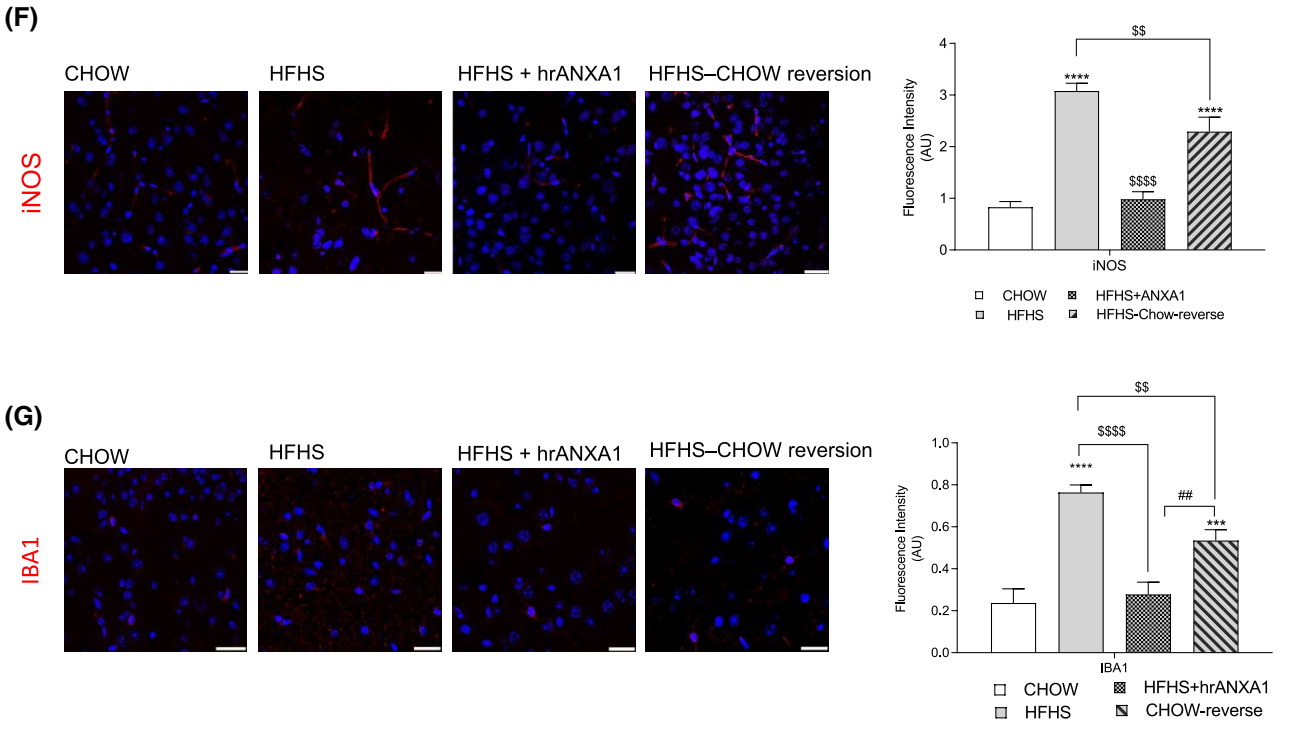
(F)
CHOW
HFHS
HFHS + hrANXA1
HFHS–CHOW reversion
iNOS
Fluorescence Intensity (AU)
$$
****
****
$$$$
iNOS
CHOW
HFHS
HFHS+ANXA1
HFHS-Chow-reverse
(G)
CHOW
HFHS
HFHS + hrANXA1
HFHS–CHOW reversion
IBA1
Fluorescence Intensity (AU)
$$
$$$$
****
##
***
IBA1
CHOW
HFHS
HFHS+hrANXA1
CHOW-reverse

FIGURE 4 Consumption of a HFHS-fed diet induces a low-grade chronic inflammatory state in the circulating serum and at the BBB. Pharmacological and dietary interventions have anti-inflammatory effects. Simultaneous measurement of multiple cytokines, chemokines, interleukins, other inflammatory markers, and metabolic markers in both serum and protein extract from brain microvessels of chow-fed, HFHS-fed, HFHS-fed + hrANXA1 treated, and HFHS—chow reversion diet mice using Mouse Cytokine Array Kits (R&D Systems). Membrane-based immunoassays detected the relative expression levels of analytes detected as arbitrary units. Analytes were measured in (A) serum ($n = 10$ pooled/group) or in (B–E) brain microvessels ($n = 10$ pooled/group, two technical replicates per experiment, performed in duplicate total $n = 20$/group) and categorized as (B) inflammatory factors, (B) chemokines, (D) pro-inflammatory interleukins, (E) anti-inflammatory interleukins. (F) Confocal microscopy of cerebral cortex sections immunostained stained for iNOS, or (G) IBA 1. Nuclei were labeled with TO-PRO3. Scale bar: 25 μm. Quantification of staining shown as mean fluorescence intensity (arbitrary units) of markers ($n = 4$ mice/group, 35 section/animal, 10 randomly selected fields/sections). Statistical analysis was performed by one-way ANOVA followed by a Bonferroni post hoc test (statistical analysis presented in Figure S3). Data are expressed as mean ± SEM. $^{*}p < .05$, $^{**}p < .01$, $^{***}p < .001$ versus chow; $^{\$}p < .05$, $^{\$\$}p < .01$ versus HFHS, $^{\#}p < .05$, $^{\#\#}p < .01$, $^{\#\#\#}p < .001$ versus HFHS + hrANXA1

they were placed in contact for 4 h with an in vitro model of the BBB, using bEnd3 cells plated on transwells to conduct a transmigration assay. The migrated cells represented those, which had crossed the BBB, whereas the adhered cells were equivalent to the immune cells that had arrested on the endothelium but had not crossed the BBB. Both adhesion and migration of $CD3^+$ $CD45^+$ T-cells were greater with lymphocytes isolated from HFHS-fed mice than those from chow-fed animals (Figure 5E) suggesting that lymphocytes isolated from HFHS-fed mice have increased migratory activity. hrANXA1 treatment in HFHS-fed mice significantly reduced the number of $CD45^+$ $CD3^+$ adhered and migrated cells when compared to the HFHS-fed mice (Figure 5E). Intriguingly, HFHS—chow reversion diet did not abolish the higher adhered or migratory numbers of $CD45^+$ $CD3^+$ cells (Figure 5E).

3.4 | Metabolic overload-induced inflammation is a key driver in the loss of BBB functionality

Macro- and micro-vascular complications are attributable to endothelial dysfunction occurring as a result of the low-grade chronic inflammation induced by hyperglycemia, dyslipidemia, and hypertensive state. We showed in Figure 4 a raise in inflammatory mediators both within the serum and at the brain microvessels in HFHS-fed mice, we, therefore, hypothesized that systemic circulating pro-inflammatory factors could contribute to the impaired BBB state observed. We investigated the effect of sera on an in vitro model of the BBB, using bEnd3 cells, and first observed an increased production of NO by cells stimulated with HFHS-fed sera compared to cells stimulated with chow-fed mice serum (Figure 6A). Serum from HFHS-fed + hrANXA1-treated and HFHS—chow reversion diet mice both produced lower levels of NO when compared to HFHS-fed mice, although this was only significant for dietary reversion (Figure 6A). Measurement of parameters of permeability and TEER (Figure 6B,C) showed disrupted BBB integrity from HFHS-fed mice serum when compared to chow-fed mice serum that was corrected with serum from HFHS-fed + hrANXA1 treated and HFHS—chow reversion mice. The in vitro results correlated with a loss of TJ protein occludin (Figure 6E), adherens junction protein VE-cadherin (Figure 6E), and the actin cytoskeleton seen through an increased G:F actin ratio (Figure 6F) in HFHS-fed mice when compared to chow-fed. We have previously shown[15] that hrANXA1 is able to restore TJ at the BBB through F-actin stabilization; here, we further confirmed our previous finding and furthermore showed that the reverse diet also restored the actin cytoskeleton through changes in the G:F ratio along with restored occludin and VE-cadherin (Figure 6D,E). Likewise, bEnd3 cells stimulated with HFHS-fed mice sera showed an increased presence of adhesion molecule ICAM-1 and co-stimulatory molecule CD86 (Figure 6F) that resulted in increased adherence/migratory capacity of $CD45^+$ $CD3^+$ leukocytes across the bEnd3 monolayer when compared to chow-fed mice (Figure 6G). Furthermore, reduction of ICAM-1 and CD86 in the intervention arms (Figure 6F), correlated with reduced adherence/migratory capacity of $CD45^+$ $CD3^+$ leukocytes when compared to HFHS-fed mice (Figure 6G). The results from these in vitro studies are comparable to the in vivo and ex vivo data shown measuring similar parameters, therefore, confirming the role played by metabolic overload-induced inflammation in BBB damage.

3.5 | Brain vascular leakage and immune cell infiltration correlate with increased MMP in T2DM patients

To corroborate whether the observations made in the mouse model can be replicated in the human disease, we investigated *post-mortem* brains from T2DM patients (described in Materials and Methods). The autoptic human cerebral cortex was double-stained for VE-cadherin/CD31 (Figure 7A) and pan-laminin/CD45 (Figure 7B). Analysis

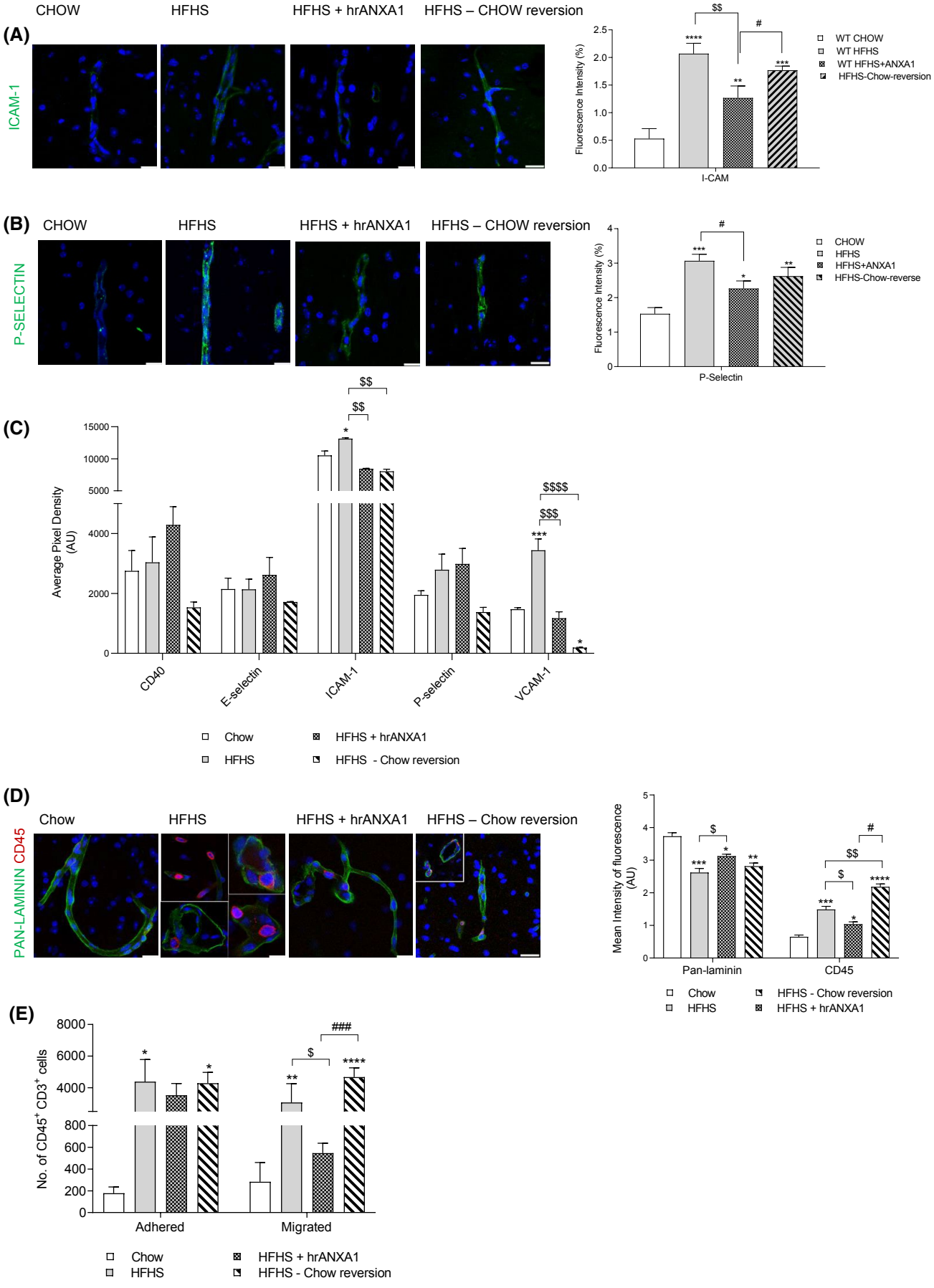
(A)
CHOW
HFHS
HFHS + hrANXA1
HFHS – CHOW reversion
ICAM-1
Fluorescence Intensity (%)
I-CAM
WT CHOW
WT HFHS
WT HFHS+ANXA1
HFHS-Chow-reversion
(B)
P-SELECTIN
P-Selectin
CHOW
HFHS
HFHS+ANXA1
HFHS-Chow-reverse
(C)
Average Pixel Density (AU)
CD40
E-selectin
ICAM-1
P-selectin
VCAM-1
Chow
HFHS
HFHS + hrANXA1
HFHS - Chow reversion
(D)
PAN-LAMININ CD45
Chow
HFHS
HFHS + hrANXA1
HFHS – Chow reversion
Mean Intensity of fluorescence (AU)
Pan-laminin
CD45
Chow
HFHS
HFHS - Chow reversion
HFHS + hrANXA1
(E)
No. of CD45+ CD3+ cells
Adhered
Migrated
Chow
HFHS
HFHS + hrANXA1
HFHS - Chow reversion

FIGURE 5 HFHS feeding induces enhanced adhesion molecule expression on BBB endothelium correlating to increased transmigration of leukocytes into the brain parenchyma, this is restored with hrANXA1 treatment. Confocal microscopy of cerebral cortex immunostained for endothelial cell adhesion molecules (A) ICAM-1 and (B) P-selectin. (C) Relative expression of adhesion molecules E-selectin, ICAM-1, P-selection and VCAM-1 and co-stimulatory molecule CD40 in brain microvessel extracts of chow-fed, HFHS-fed, HFHS-fed + hrANXA1-treated, and HFHS—chow reversion diet mice ($n = 10$ pooled/group, two technical replicates per experiment, performed in duplicate total $n = 20$/group) using a membrane-based immunoassay (R&D Systems). (D) Double immune-cortical staining for leukocyte marker CD45 and pan-laminin. Nuclei were labeled with TO-PRO3. Scale bar: 25 μm. Quantification of staining shown as mean fluorescence intensity (arbitrary units) of markers ($n = 4$ mice/group, 35 section/animal, ten randomly selected fields/sections). (E) Isolated mouse lymphocytes from cervical lymph nodes of chow-fed, HFHS-fed, HFHS-fed + hrANXA1-treated, and HFHS—chow reversion diet-fed mice, were placed in contact on transwells with bEnd3 cells for 4 h ($n = 5$–9/group). Adhered populations of leukocytes were collected from the transwell, the upper compartment, and migrated cells were collected from the bottom compartment. Flow-activated cell staining was used to evaluate firm adhesion and transmigration of $CD3^+$ T-cells expressing $CD45^+$, plot gate and strategy are shown for both adhesion and migration. Statistical analysis was performed by one-way ANOVA followed by a Bonferroni post hoc test. Data are expressed as mean ± SEM. $^*p < .05$, $^{**}p < .01$, $^{***}p < .001$, $^{****}p < .0001$ versus chow; $^{\$}p < .01$, $^{\$\$}p < .01$, $^{\$\$\$}p < .001$, $^{\$\$\$\$}p < .0001$ versus HFHS; $^{\#}p < .01$, $^{\#\#}p < .01$, $^{\#\#\#}p < .001$, $^{\#\#\#\#}p < .0001$ versus HFHS + hrANXA1

showed a slight but significant reduction of VE-cadherin and CD31 immunostaining in microvessels of T2DM patients, paralleled by laminin reduction in the VBL (Figure 7A,B). Additionally, $CD45^+$ immune cells were more numerous and strongly immunoreactive in T2DM patients compared with healthy controls (Figure 7B). Together, these results parallel the disruption seen to tight junctions and vessel basal lamina components in mice that resulted in leukocyte transmigration into the mouse brain parenchyma (Figures 1 and 4).

As our mouse in vitro model showed that systemic circulating soluble factors can affect the integrity of the BBB, we conducted a similar investigating using a humanized in vitro BBB model with a human cerebral microvascular endothelial cell line, hCMEC/D3.[4] Cells were stimulated with sera from healthy donors (HD) or T2DM patients (Table S1). Stimulation with T2DM sera resulted in a leaky BBB phenotype according to both analyzed parameters of paracellular permeability and TEER (Figure 7C,D); disruption to BBB function could be attributed to the decreased expression of junctional proteins occludin and VE-cadherin (Figure 7E). Additionally, the expression of ICAM-1 was upregulated in cells stimulated with T2DM patient serum compared to HD serum, implicating the potential for the leukocyte transmigration (Figure 7F). Analysis of T2DM patient serum indicated raised levels of the pro-inflammatory cytokines, TNF-α and IL-6 (Figure 7G) that could be responsible for the observed change. Furthermore, stimulation of hCMEC/D3 cells with HD or T2DM donor sera resulted in an increase of MMP-9 and MMP-13 expression in T2DM patients versus HD (Figure 7H). Within the serum of T2DM patients, the TIMP-2 levels declined compared to HD (Figure 7I). Overall, the results from the human in vitro model showed similar disruption to BBB integrity with T2DM serum stimulation as was seen in HFHS-fed mice.

4 | DISCUSSION

Endothelial cells serve as a key interface between the blood and organs; therefore, vascular health is a key determinant in disease progression. The endothelium of the brain in particular is exquisitely specialized to protect the brain from blood-borne inflammation and ensure brain homeostasis. Disruption of the BBB has been closely linked with cognitive impairment in a wide range of conditions, including Alzheimer's disease,[40] Parkinson's disease,[5] and T2DM.[41] Here, we show that the metabolic overload and associated systemic, low-grade inflammation directly impairs BBB integrity, suggesting that the cerebral vasculature is an important pathological target, even in the absence of overt disease. Notably, either dietary approach via a diet reversion or a pharmacological approach via administration of the anti-inflammatory protein hrANXA1 can in part reverse both the endothelial and inflammatory changes induced by a HFHS diet.

Metabolic overload impairs BBB function by increasing paracellular permeability and decreasing TEER, changes attributable to the loss of TJ proteins occludin and claudin-5 and VBLs. It has been demonstrated that laminin α2 null mice have a defective BBB, with leakage of the injected exogenous tracers, and the lack of expression of laminin 2 subunit is paralleled by molecular defects at the endothelium VBL layer.[42] Under physiological conditions, laminin α2 is expressed by astrocytes and pericytes[28,43,44] and its expression in astrocyte end-feet coincides with astrocyte-pericyte sites of interaction, which in turn are involved in cellular communication and BBB structural integrity.[45] Considering that pericytes are also in charge of immune mediator release and regulation of leukocyte transmigration, and altered astrocyte-pericyte cross-talk may also participate in the neuroinflammatory processes.[46,47]

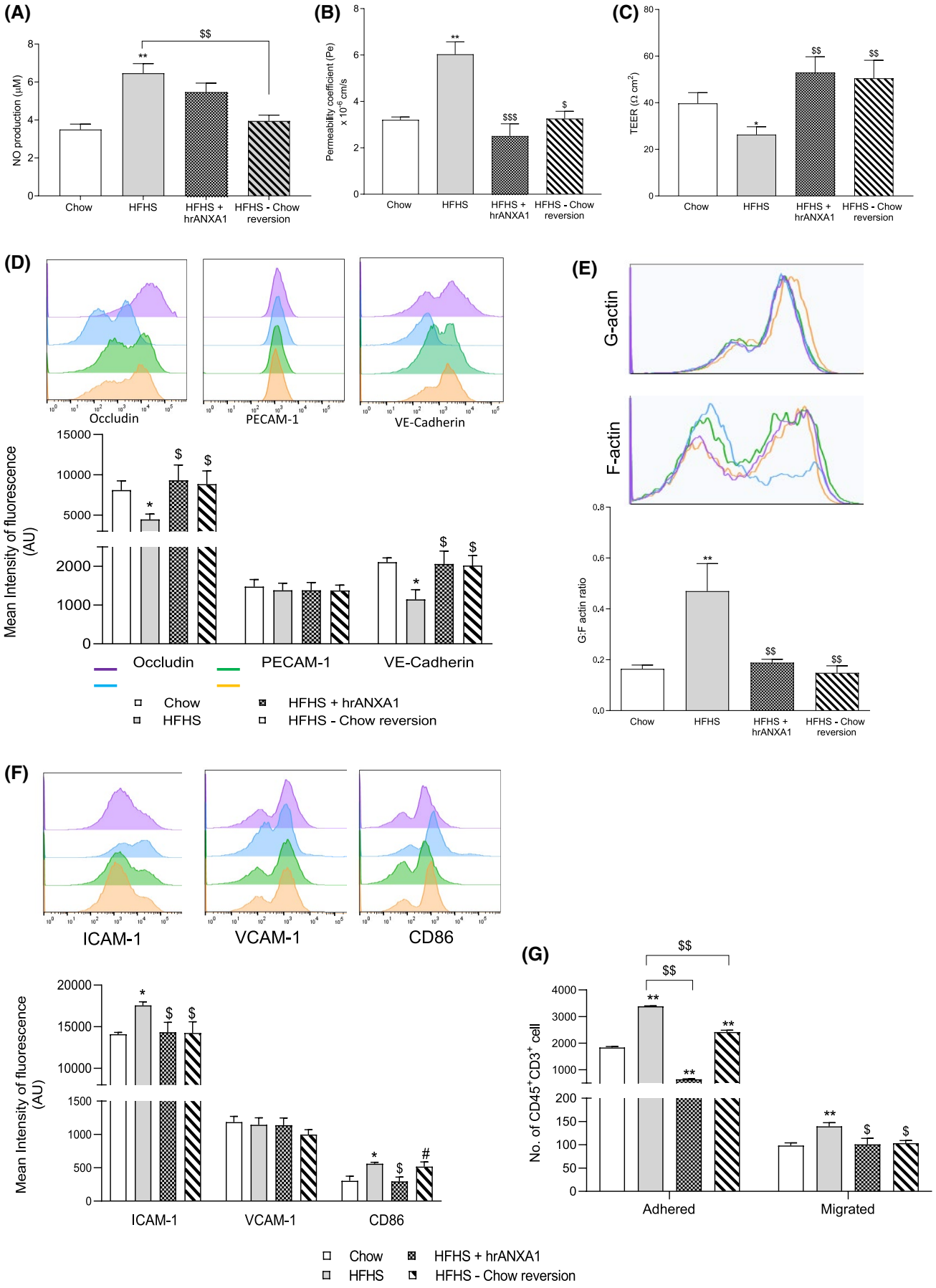
(A)
NO production (μM)
Chow
HFHS
HFHS + hrANXA1
HFHS - Chow reversion
(B)
Permeability coefficient (Pe) x 10⁻⁶ cm/s
(C)
TEER (Ω cm²)
(D)
Occludin
PECAM-1
VE-Cadherin
Mean Intensity of fluorescence (AU)
(E)
G-actin
F-actin
G:F actin ratio
(F)
ICAM-1
VCAM-1
CD86
(G)
No. of CD45⁺CD3⁺ cell
Adhered
Migrated

FIGURE 6 Mouse serum significantly disrupts BBB function in vitro, correlating to in vivo results. Sera (10%) from mice—chow-fed, HFHS-fed, HFHS-fed + hrANXA1 treated and HFHS—chow reversion diet fed, were used to stimulate mouse brain endothelial cells, bEnd3 monolayers for 16 h unless otherwise stated. (A) Production of nitric oxide (NO) from brain endothelial cells bEnd3 after stimulation for 6 h. Measurement of (B) paracellular permeability coefficients to 70 kDA FITC-dextran and (C) transendothelial electrical resistance (TEER) ($n = 30$/group, 10 pooled/group per independent experiments). Flow cytometric analysis of (D) junctional proteins occludin, PECAM-1 & VE-cadherin (E) G:F actin ratio and (F) adhesion molecules ICAM-1, VCAM-1, and CD86 ($n = 6$–26/group, pooled in pairs, 3 independent experiments) expressed as mean intensity of fluorescence values. Isolated mouse lymphocytes from cervical lymph nodes of chow mice were placed in contact on transwells with bEnd3 cells and stimulated with mouse serum for 4 h. Adhered cell populations were collected from the upper compartment, and migrated cells were collected from the bottom compartment. (G) Flow activated cell staining was used to evaluate firm adhesion and transmigration of $CD3^+$ $CD45^+$ leukocytes (pool 10 mice sera/group, on 6 pooled cervical lymph nodes T cells expanded, see material and methods section). Statistical analysis was performed by one-way ANOVA followed by a Bonferroni post hoc test. Data are expressed as mean ± SEM. $^*p < .05$, $^{**}p < .01$. $^{***}p < .01$ versus chow; $^{\$}p < .05$, $^{\$\$}p < .01$, $^{\$\$\$}p < .001$, versus HFHS; $^{\#}p < .05$ vs HFHS + hrANXA1

The laminin subunits of the endothelial VBL layer are regulated in part by MMP activity, helping to maintain normal tissue homeostasis, this process is known to be dysregulated in a number of CNS diseases, including MS, AD, stroke, and glioma.[32,48] MMP activity is transcriptionally regulated by, among others, cytokines, and ROS,[32–34] which may be relevant in the context of the low-grade, chronic, and non-resolving inflammation[49] known to be present in T2DM and which was observed in HFHS-fed mice. The activity of MMPs is further regulated by the presence and action of TIMPs[33,34]; hence, the maintenance of efficient BBB function requires a balance between MMP and TIMP expression. In HFHS-fed mice, TIMP-1 activity was significantly reduced in comparison to chow-fed mice, in combination with raised MMP-2 and MMP-9 activity, indicating a potential disruption in the balance and control of MMP activity.

Numerous studies have reported pro-inflammatory IL-1α and TNF-α as upregulating TIMP-1 levels in both endothelial cells and astrocytes.[50,51] In mouse models of experimental encephalomyelitis (EAE), GFAP-expressing astrocytes increase TIMP-1 expression to aid remodeling of the brain ECM.[52] Similarly, in the human T-lymphotropic virus, T_H1 cells interact with astrocytes causing them to become reactive; reactive astrocytes secrete pro-inflammatory cytokines and express TIMP-1 and TIMP-3.[53] Although in our diabetic model, there is a substantial increase in the presence of T-cell inducing chemokines, the serum and brain microvessel protein levels of TIMP-1 are decreased. This contrast, between our results and other studies[53] showing upregulated TIMP-1, may in fact represent the switch between a protective vs detrimental effect of MMPs/TIMPs.

However, differential regulation of TIMP-1, specifically in astrocytes of AD patients, correlates with acute vs chronic inflammatory state of the disease.[54,55] In inflammation, astrocytes initially become activated to serve as a protective mechanism, isolating the damaged area and facilitating brain circuit remodeling.[6] As such, acute activation of astrocytes along with microglial activation may enhance the levels of TIMP-1 in the brain microenvironment to allow positive remodeling. However, under sustained inflammation, the levels of TIMP-1 cannot be maintained and, therefore, decline significantly. In a similar manner, in the diabetic mouse model where there is underlying chronic inflammation, the results show an imbalance of TIMP-1 and MMPs. In fact, a study of T2DM patients found serum concentrations of MMP-2 and MMP-9 to be lower in diabetic patients vs non-diabetic controls during short-lasting hyperglycemia induced by oral glucose tolerance test, whereas chronic hyperglycemia, reflected by glycated hemoglobin levels, correlated with higher MMP-9 levels in T2DM patients.[56] Such published data are in line with our human serum studies, we find diabetic patients to have increased MMP-9.

A critical component of T2DM is the low-grade chronic inflammation that is characterized by cytokine expression and immune cell infiltration that remains unresolved over time.[42] In metabolic disorders, excessive nutrient consumption leading to hyperglycemia and dyslipidemia is accompanied by a plethora of inflammatory and metabolic responses in multiple cell types and is termed meta-flammation, i.e., metabolism-induced inflammation.[43,44] Although peripherally-originating leukocytes and dendritic cells are occasionally detected in the perivascular compartment as components of the immune surveillance machinery, the number of these cells in the brain is typically restricted compared to those seen in peripheral organs.[57,58] The presence of few perivascular $CD45^+$ cells (i.e., leukocytes) scattered in the cortex of HFHS-fed mice, may suggest a possible easier passage of immune cells into the brain parenchyma, and consequent activation of microglia cells as depicted by our Iba1 immunostaining. However cellular source of hypothalamic macrophages accumulation has been reported in diet-induced obesity, though the mechanism is still unclear.[59] Importantly, disruption of the BBB alone is not sufficient to result in leukocyte transmigration into the CNS parenchyma,[60] rather there appears to be a need for locally-derived cues, such as inflammatory activity.[61] Several events are required to

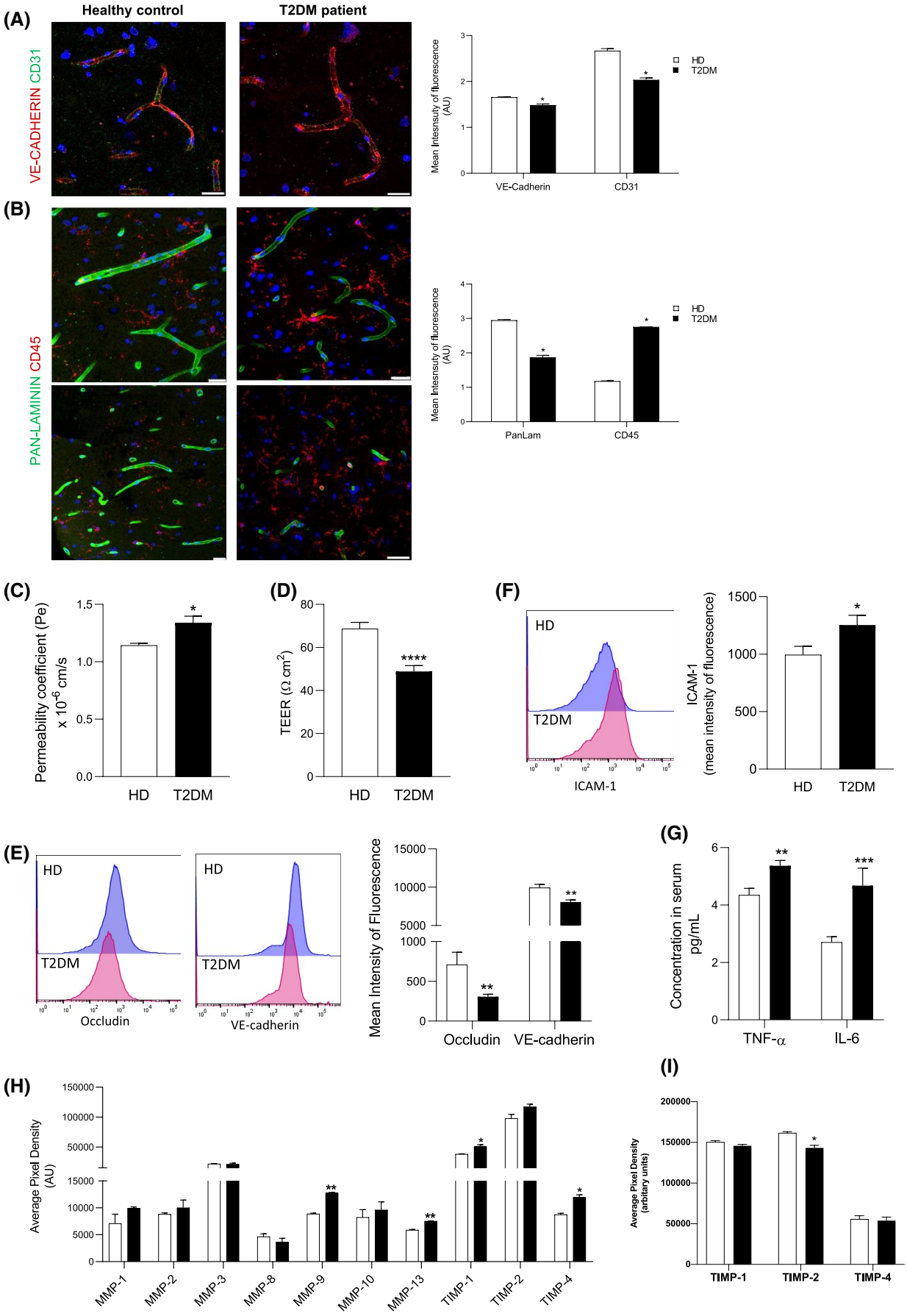
(A)
Healthy control
T2DM patient
VE-CADHERIN CD31
Mean Intesnsuty of fluorescence (AU)
HD
T2DM
VE-Cadherin
CD31
(B)
PAN-LAMININ CD45
PanLam
CD45
(C)
Permeability coefficient (Pe) x 10-6 cm/s
(D)
TEER (Ω cm2)
(E)
Occludin
VE-cadherin
Mean Intensity of Fluorescence
(F)
ICAM-1
(mean intensity of fluorescence)
(G)
Concentration in serum pg/mL
TNF-α
IL-6
(H)
Average Pixel Density (AU)
MMP-1
MMP-2
MMP-3
MMP-8
MMP-9
MMP-10
MMP-13
TIMP-1
TIMP-2
TIMP-4
(I)
Average Pixel Density (arbitary units)

FIGURE 7 Patients with T2DM present with brain vascular leakage and immune cell infiltration and serum from T2DM patients also significantly disrupt BBB function. Post-mortem brain sections of health donor (HD) and T2DM patients immuno-stained for (A) VE-Cadherin/CD31 and (B) pan-laminin/CD45. Nuclei were labeled with TO-PRO3. Scale bar: 25 μm. Quantification of staining shown as mean fluorescence intensity (arbitrary units) of markers ($n = 4$ patients/group, 35 section/patient, 10 randomly selected fields/sections). Sera (20%) from healthy donors or T2DM patients was used to stimulate human brain endothelial cells hCMEC/D3 monolayers for 16 h. Measurement of (C) paracellular permeability coefficients and (D) transendothelial electrical resistance (TEER), ($n = 12$ donors/group, pooled in pairs matched in sex and age). (E) Flow cytometric analysis of junctional proteins occludin and VE-cadherin and (F) ICAM-1 ($n = 12$ donors/group, pooled in pairs matched in sex and age). (G) Concentration of TNF-α and IL-6 measured in the serum of HD or T2DM patients using a multiplex ELISA ($n = 19–28$/group, age and sex-matched). (H) Relative expression of MMPs measured in hCMEC/D3 cells ($n = 10$ pooled/group) (I) Relative expression of TIMPs in sera of HD or T2DM patients ($n = 10$ pooled/group). Statistical analysis was performed by either an independent Student's *t*-test or Mann–Whitney *U* test. Data are expressed as mean ± SEM. $^{*}p < .05$, $^{**}p < .01$, $^{***}p < .001$, $^{****}p < .0001$ vs HD

permit the migration of leukocytes across an endothelium barrier. First and foremost, chemokine signals induce the chemotaxis of immune cells, i.e., cell adhesion molecules such as ICAM-1, P-, and E-selectin is required in the brain microvasculature itself.[59] Notably, we found that consumption of a HFHS diet enhanced expression of both chemokines and cell adhesion molecules in the cerebral microvasculature compared to chow-fed mice and that these changes were attenuated, although not fully reversed, by either diet reversion or hrANXA1 treatment, further emphasizing the ability of both interventions to protect the CNS environment through reduction of chronic inflammation and repair of the cerebral vasculature.

Due to the tightly regulated nature of the brain microenvironment, the transmigration of leukocytes across the BBB into the brain parenchyma is in fact a two-step process.[62–64] To cross into the brain parenchyma, the invading cells must be able to cross both the inner endothelial BM and the outer astrocytic BM. In the HFHS-fed mice, double immunostaining with pan-laminin (a marker for both endothelial and astrocytic BM) and the general leukocyte marker CD45 shows clear entrapment of $CD45^+$ leukocytes between the two BM layers, the perivascular space, with limited infiltration into the brain parenchyma itself, a feature not seen in chow-fed mice. Initial passage across the endothelial cells requires an integrin-adhesion molecules-mediated process. As noted, the number of adhered/migrated leukocytes was far greater in the HFHS-fed T2DM model indicating that these cells were interacting with adhesion molecules to allow the transmigration cascade. Moreover, activated leukocytes also release MMPs to aid in passage across the BBB.[48,65] The production of MMPs by tissue and immune-cell sources is believed to be strongly affected by cytokine levels. Work by Sorokin and colleagues show that the balance of TNFα vs IFNγ regulates activation of astrocytes and secretion of MMP-9.[64] Interestingly, in the HFHS-diet model, there is an increase of both TNFα and IFNγ at the brain microvessels; especially the relative expression of TNFα to IFNγ is much higher.

The findings in vivo/ex vivo correlates with the in vitro BBB model where bEND3 cells treated with HFHS-fed mice serum resulted in increased paracellular permeability and reduced TEER compared with chow-fed mice serum-stimulated cells, which can be accounted for the reduction of junctional proteins such as occludin and VE-cadherin as well as loss of the actin filamentous fibers. Moreover, the HFHS-fed mice serum activates the bEnd3 cells to upregulate adhesion molecule expression. In addition, cells stimulated with HFHS-fed mice serum show an upregulation of co-stimulatory molecule CD86, indicating that the brain endothelial cells themselves act as antigen-presenting cells under inflammatory stimuli, as previously reported.[45,46] This coincides with the increased adhesion and migratory profile of $CD45^+$ leukocytes.

Confirmation of the role of inflammatory mediators in inducing BBB damage, allowed us to corroborate our results into a humanized in vitro BBB model using hCMED/3 cells stimulated with serum from T2DM patients or healthy donors. A number of studies have reported correlations between high peripheral inflammation and risk of neurodegenerative diseases such as AD, PD, HD, ALS, and MS.[47,48] Here, we showed raised TNF-α and IL-6 in T2DM patient sera resulted in junctional protein (occludin and VE-cadherin) loss contributing to a leaky BBB phenotype. Observations in human post-mortem brain confirmed the reduction of VE-cadherin and CD31 in microvessels of T2DM patients, paralleled by laminin reduction in the VBL. As with the mouse model, loss of the BBB structure corresponded with increased $CD45^+$ leukocytes in the brain parenchyma of T2DM patients compared with healthy controls. BBB barrier disruption coupled with CNS leukocyte infiltration has been reported to drive CNS disorders of AD, MS, and PD.[66] Furthermore epidemiological studies have long reported metabolic disorders to be a risk factor for cognitive decline[67,68] and the development of dementias.[51,52] Degenerating neurons have been observed in the cortex and hippocampal regions of rodents fed a high-fat and high-fructose diet for 24 weeks led to impaired spatial learning and memory, as tested using the Morris Water

Maze test.[69] In the past decade, there have been studies investigating the link between T2DM and AD pathology with similarities reported in the vascular pathologies between mice fed a western diet and 3× transgenic AD mice for development of peripheral insulin resistance, accumulation of Aβ and phosphorylated tau, and behavioral and cognitive abnormalities.[70–72] The results of our study implicate the pathophysiological changes occurring at the BBB arising from a peripheral metabolic disease that can lead to the development of these neurovascular diseases. The simultaneous rise of pro- and anti-inflammatory mediators activate and alter multiple signaling cascades[73–76] and it can be hypothesized that BBB breakdown in T2DM will alter the brain microenvironment to propagate a vicious cycle of self-propelling inflammation from brain endothelial cells, astrocytes, microglia and neurons that ultimately lead to chronic neuroinflammation and neurodegeneration.[77] Investigation into neuronal loss is beyond the scope of this study; however, future studies would benefit from reviewing the effect on neurons and subsequent cognitive behaviors, with particular focus on whether BBB improvement in pharmacological and dietary interventions can translate to the restoration of the cognitive abnormalities induced by high-fat feeding reported in other studies.[78]

It has long been established that T2DM can cause microvessel damage in the peripheral system resulting in secondary complications such as retinopathy and neuropathy.[79] The restoration of BBB integrity and functionality with hrANXA1 treatment or a dietary change implicates that damage the brain microvasculature is also a secondary complication of T2DM-induced metaflammation.

The benefits of ANXA1 as a therapeutic agent have long been investigated. We have previously demonstrated that ANXA1$^{-/-}$ mice fed a HFHS diet have a more severe diabetic phenotype compared to wild-type HFHS-fed mice, with severe dyslipidemia, hepatic steatosis, and renal dysfunction.[16] Other studies using LDLR$^{-/-}$ mice have shown hrANXA1 treatment to reduce atherosclerotic plaque burden and improve plaque stability through reduced lipid accumulation,[80] demonstrating the therapeutic benefit of ANXA1 in treating metabolic disease and its associated peripheral co-morbidities. Arguably, ANXA1's best therapeutic effects are known at the BBB. ANXA1 has been shown to improve tight junction stability through restoring F-actin organization via co-localization with β-actin,[15] inhibition of leukocyte TEM through inducing L-selectin shedding from leukocytes to prevent tethering, rolling, and firm adhesion[81] and through co-localization with α4β1 integrin on leukocytes to prevent binding to VCAM-1 on endothelium.[82] Here, we extend our findings of the therapeutic effect of hrANXA1 treatment also on the essential components of the BM; with the clear restoration of endothelial and astrocytic laminin α4 and laminin α2, respectively. This allowed for the re-attachment of astrocytic end-feet to the brain endothelial cells to restore the full structure of the BBB in HFHS-fed + hrANXA1-treated mice that contributed to the reduced infiltration of CD45^{+} into the brain parenchyma. Within the brain, ANXA1 has been shown to contribute to microglia surveillance and maintenance of brain homeostasis through reducing the phagocytosis of non-apoptotic neurons under inflammatory conditions and reducing the production of NO from microglia cells[83] along with promoting the transition of activated microglia from an M1 to M2 phenotype through peptide-FPR engagement.[74] In our study, we find hrANXA1 treatment in HFHS-feeding reduced Iba1^{+}-activated microglia presence and reduced iNOS expression/NO production.

It is well recognized that an improved diet can help control and manage T2DM and the development of CVDs[84–88] and there is growing evidence of the role of Mediterranean and dietary approaches to stop hypertension (DASH) diets in reducing cognitive decline and lowering AD risk.[89] However, the majority of these studies are large longitudinal observation studies or meta-analyses. To our knowledge, our study is the first to examine the effect of diet on the structural and functional changes of the brain microvasculature in a diabetic model induced by HFHS-feeding. From the results, it is clearly noticeable that dietary changes have a huge impact on BBB integrity with significantly reduced Evans blue dye extravasation, reduced paracellular permeability of FITC-dextran, and increased TEER compared to HFHS-fed mice. Reduced leakage can be accounted for the restoration of junctional proteins; although while occludin presence at junctional sites is beginning to be re-established, the laminin reactivity remains low preventing the ensheathment of astrocytes. As a result of the lack of complete BBB restoration, in the HFHS—chow reversion diet mice CD45^{+} leukocytes are still present within the VBL layers and appear to show migration outwards into the brain parenchyma. These results together illustrate that brain endothelial cells contacts are repaired with dietary changes, however, the BBB vasculature in its entirety is not restored. This may be due to the length of time in which dietary reversion occurred (five weeks), which may not be sufficient to fully recover from the HFHS insult and further studies will be needed to address this. Studies that have investigated dietary changes in diabetic rodents by food or calorie restriction,[90–92] ketogenic diets,[93] herbal formulas,[94] reduced glycoxidation products,[95] or addition of extra virgin olive oil[96] report improved insulin sensitivity with feeding over a duration of 8–24 weeks on intervention. In our study, a 5-week intervention begins to improve insulin and lipid levels, however, optimal glycemic control has not been achieved, however, there is a significant reduction

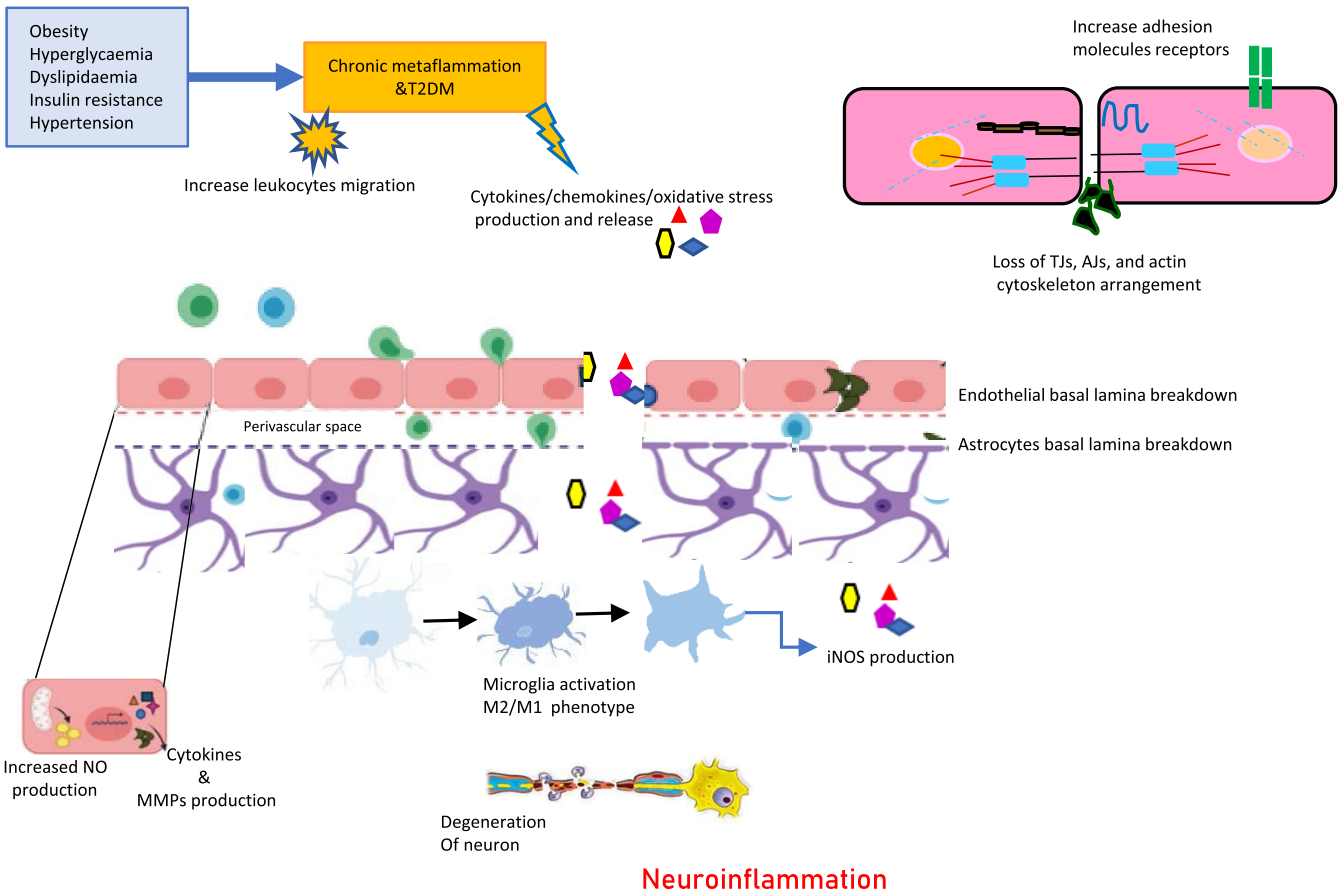

FIGURE 8 Schematic representation of the effect of HFHS-feeding on BBB structure and functionality, leading to neuroinflammation. The traits of metabolic disorders—obesity, hyperglycemia, dyslipidemia, insulin resistance, and hypertension, create a low-grade chronic inflammatory state termed metaflammation which results over time in the development of T2DM. Chronic metaflammation is responsible for producing a number of cytokines, chemokines, and oxidative stress as well as activating the immune system. The damage by inflammation and the immune system leads to a leaky BBB phenotype that can be correlated to the loss of TJs and AJs, the actin cytoskeleton, and the loss of basal lamina α4 on endothelial cells and α2 astrocytic end-feet. This breakdown is mediated by the imbalance of MMPs/TIMPs and results in complete loss of the BBB structure with the dissociation of the astrocytes to the blood vessel. The accumulation of inflammatory mediators and oxidative stress contributes to the production of these MMPs. Increased adhesion molecule expressions along with BBB dysfunction resulted in increased transendothelial migration of leukocytes into the brain parenchyma. Microglia become activated. It is hypothesized that the astrocytes, microglia, and neurons also sense changes in the brain microenvironment and are likely to respond to the increased presence of inflammatory mediator passage by further up-regulating the release of cytokines, chemokines, MMPs, and ROS production that triggers pro-inflammatory signaling pathways. These events together are, therefore, likely to create a self-destructing environment within the brain triggering neuroinflammation and subsequent neuronal destruction. Some objects/images have been extracted from the web

in metaflammation. The benefit of Mediterranean diets, rich in polyunsaturated fats, flavonoids, vitamins, and minerals (calcium, iron, zinc, etc.), are associated to the high presence of omega-3 fatty acids, antioxidants, and polyphenols that reduce free radical generation and cytokine production, thereby inhibiting pro-inflammatory signaling pathways[97,98] that lead to improved cognition and learning by facilitating synaptic plasticity and/or enhancing synaptic membrane fluidity through reduction of inflammation and oxidative stress.[98–100] At this stage, we can speculate that dietary reversion, through its effect on inflammatory mediators, might benefit BBB function, but this remains a topic for future investigation.

Evaluating both interventions, it appears that ANXA1 has more direct effects on the BBB restoration, through its links with the actin cytoskeleton, basal lamina, and TEM prevention. On the contrary, the attributes of a healthy diet are through reduced inflammatory mediators, downstream this would result in the altering of signaling pathways associated with T2DM. It can, therefore, be hypothesized that a combination of hrANXA1 treatment with dietary reversion would result in greatly improved T2DM outcomes both in the peripheral and central systems.

In conclusion, our study demonstrates that a HFHS-dietary intake in mice or T2DM in patients causes microvascular complications at the BBB (Figure 8). The

growing obesity and T2DM epidemic, therefore, raise concerns for the potential pathogenesis of neurodegenerative brain disorders and cognitive decline on top of the well-known macrovascular and microvascular complications T2DM. The need for innovative approaches to healthcare is paramount and the ability of hrANXA1 and dietary intervention to reduce and restore the metabolic triggered inflammation-induced BBB damage provides hope for ways we can slow down T2DM-associated neuroinflammation.

ACKNOWLEDGMENTS

We would like to thank the following funding bodies for their support: the British Heart Foundation (Grant/Award number: FS 16/60/32739) to M.H.S.; Ministry of Education-CAPES, Brazil (Grant number: 7326/2014-09) to R.A.L.; "Cibo, Microbiota, Salute" by "Vini di Batasiolo S.p.A" AL-RIC19ABARA_01 to A.B.; "Post-Doctoral Fellowship 2020" by "Fondazione Umberto Veronesi" 2020-3318 to A.B.; Fondazione Cariplo 2016-0852 to G.D.N.; EFSD/Lilly European Diabetes Research Programme 2018 to G.D.N.; Fondazione Telethon GGP19146 to G.D.N.; PRIN 2017K55HLC to G.D.N.; Fondazione Cariplo 2015-0524 and 2015-0564 to A.L.C.; H2020 REPROGRAM PHC-03-2015/667837-2 to A.L.C.; Ministero della Salute GR-2011-02346974 to A.L.C.; ERA NET ER-2017-2364981 to A.L.C.; PRIN 2017H5F943 to A.L.C.; FISM Fondazione Italianana Sclerosi Multipla (Cod. 2014/R/21) to E.S.

DISCLOSURES

The authors state that there are no conflicts of interest in connection with this article.

AUTHOR CONTRIBUTIONS

Madeeha H. Sheikh performed experiments as part of her PhD thesis, analyzed, and interpreted the data, and contributed to the manuscript writing. Mariella Errede designed the experimental for confocal studies and contributed to confocal and morphometric data discussion. Antonio d'Amati performed experiments as part of his Medical degree thesis, executed, and analyzed immunostaining, and confocal microscopy, on both mouse and human brains, and morphometrically quantified the data. Noorafza Q. Khan performed the western blots and assisted with the zymography. Silvia Fanti performed transmigration experiments; Simon McArthur assisted with the zymography and contributed to the writing and discussion of the paper. Rodrigo A. Loiola and Gareth S. D. Purvis performed the Evans blue experiment. Caroline E. O'Riordan and Julius Kieswich provided technical assistance with animal work. Chis Reutelingsperger provided the purified hrANXA1. Giuseppe Danilo Norata, Andrea Baragetti, and Alberico Luigi Catapano provided the human samples and all the biochemical data for the study and contributed to the discussion of the manuscript; Davide Ferorelli, Alessandro Dell'Erba, and Eugenio Maiorano provided brain human samples; Magdi Yaqoob and Christoph Thiemermann provided assistance with the animal license. Federica Marelli-Berg contributed to results discussion and manuscript writing. Daniela Virgintino collected human brain samples and contributed to their analysis and discussion of the manuscript. Egle Solito designed the experiments, performed some experiments, interpreted, analyzed data, and wrote the manuscript. All authors reviewed and approved the manuscript.

ORCID

Egle Solito https://orcid.org/0000-0001-5279-0049

REFERENCES

1. Rochlani Y, Pothineni NV, Kovelamudi S, Mehta JL. Metabolic syndrome: pathophysiology, management, and modulation by natural compounds. *Ther Adv Cardiovasc Dis*. 2017;11:215-225.
2. Panza F, Frisardi V, Capurso C, et al. Metabolic syndrome and cognitive impairment: current epidemiology and possible underlying mechanisms. *J Alzheimer's Dis*. 2010;21:691-724.
3. Frisardi V, Solfrizzi V, Capurso C, et al. Is insulin resistant brain state a central feature of the metabolic-cognitive syndrome? *J Alzheimer's Dis*. 2010;21(1):57-63.
4. Sheikh MH, Henson SM, Loiola RA, et al. Immuno-metabolic impact of the multiple sclerosis patients' sera on endothelial cells of the blood-brain barrier. *J Neuroinflammation*. 2020;17(153):1-19.
5. Janelidze S, Hertze J, Nägga K, et al. Increased blood-brain barrier permeability is associated with dementia and diabetes but not amyloid pathology or APOE genotype. *Neurobiol Aging*. 2017;51:104-112.
6. Pekny M, Nilsson M. Astrocyte activation and reactive gliosis. *Glia*. 2005;50:427-434.
7. Ransohoff RM, Perry VH. Microglial physiology: unique stimuli, specialized responses. *Annu Rev Immunol*. 2009;27:119-145.
8. Rosenberg GA, Wallin A, Wardlaw JM, et al. Consensus statement for diagnosis of subcortical small vessel disease. *J Cereb Blood Flow Metab*. 2016;36:6-25.
9. Wang F, Cao Y, Ma L, Pei H, Rausch WD, Li H. Dysfunction of cerebrovascular endothelial cells: prelude to vascular dementia. *Front Aging Neurosci*. 2018;10(376):1-23.
10. Moran C, Phan TG, Chen J, et al. Brain atrophy in type 2 diabetes: regional distribution and influence on cognition. *Diabetes Care*. 2013;36:4036-4042.
11. Pannacciulli N, Del Parigi A, Chen K, Le DSNT, Reiman EM, Tataranni PA. Brain abnormalities in human obesity: a voxel-based morphometric study. *NeuroImage*. 2006;31:1419-1425.
12. van Bloemendaal L, Ijzerman RG, ten Kulve JS, et al. Alterations in white matter volume and integrity in obesity and type 2 diabetes. *Metab Brain Dis*. 2016;31:621-629.
13. Kanoski SE, Davidson TL. Different patterns of memory impairments accompany short- and longer-term maintenance on a high-energy diet. *J Exp Psychol Anim Behav Process*. 2010;36:313-319.

14. Murray AJ, Knight NS, Cochlin LE, et al. Deterioration of physical performance and cognitive function in rats with short-term high-fat feeding. *FASEB J*. 2009;23:4353-4360.
15. Cristante E, McArthur S, Mauro C, et al. Feature article: identification of an essential endogenous regulator of blood-brain barrier integrity, and its pathological and therapeutic implications. *Proc Natl Acad Sci USA*. 2013;110:832-841.
16. Purvis GSD, Collino M, Loiola RA, et al. Identification of AnnexinA1 as an endogenous regulator of RhoA, and its role in the pathophysiology and experimental therapy of type-2 diabetes. *Front Immunol*. 2019;10(571):1-16.
17. Montesano R, Pepper MS, Möhle-Steinlein U, Risau W, Wagner EF, Orci L. Increased proteolytic activity is responsible for the aberrant morphogenetic behavior of endothelial cells expressing the middle T oncogene. *Cell*. 1990;62:435-445.
18. Weksler B, Romero IA, Couraud PO. The hCMEC/D3 cell line as a model of the human blood brain barrier. *Fluids Barriers CNS*. 2013;10(16):1-10.
19. Dehouck MP, Jolliet-Riant P, Bree F, Fruchart JC, Cecchelli R, Tillement JP. Drug transfer across the blood-brain barrier: correlation between in vitro and in vivo models. *J Neurochem*. 1992;58:1790-1797.
20. Norata GD, Garlaschelli K, Ongari M, Raselli S, Grigore L, Catapano AL. Effects of fractalkine receptor variants on common carotid artery intima-media thickness. *Stroke*. 2006;37:1558-1561.
21. Ludovica Fracanzani A, Pisano G, Consonni D, et al. Epicardial adipose tissue (EAT) thickness is associated with cardiovascular and liver damage in nonalcoholic fatty liver disease. *PLoS One*. 2016;11(9):e0162473.
22. Association AD. Standards of medical care in diabetes-2011. *Diabetes Care*. 2011;34:S11.
23. Friedewald WT, Levy RI, Fredrickson DS. Estimation of the concentration of low-density lipoprotein cholesterol in plasma, without use of the preparative ultracentrifuge. *Clin Chem*. 1972;18:499-502.
24. Fuyan S, Jing L, Wenjun C, et al. Fatty liver disease index: a simple screening tool to facilitate diagnosis of nonalcoholic fatty liver disease in the Chinese population. *Dig Dis Sci*. 2013;58:3326-3334.
25. Thibault L. Animal models of dietary-induced obesity. *Anim Model Study Hum Dis*. 2013;277-303.
26. Hayden M, Grant D, Aroor A, DeMarco V. Ultrastructural remodeling of the neurovascular unit in the female diabetic db/db model—Part I: astrocyte. *Neuroglia*. 2018;1:220-244.
27. Al-Goblan AS, Al-Alfi MA, Khan MZ. Mechanism linking diabetes mellitus and obesity. *Diabetes Metab. Syndr Obes Targets Ther*. 2014;7:587-591.
28. Agrawal S, Anderson P, Durbeej M, et al. Dystroglycan is selectively cleaved at the parenchymal basement membrane at sites of leukocyte extravasation in experimental autoimmune encephalomyelitis. *J Exp Med*. 2006;203:1007-1016.
29. Yousif LF, Di Russo J, Sorokin L. Laminin isoforms in endothelial and perivascular basement membranes. *Cell Adhes Migr*. 2013;7:101-110.
30. Brew K, Nagase H. The tissue inhibitors of metalloproteinases (TIMPs): an ancient family with structural and functional diversity. *Biochim Biophys Acta—Mol Cell Res*. 2010;1803:55-71.
31. Nagase H, Murphy G. Tailoring TIMPs for selective metalloproteinase inhibition. In: Edwards D, Høyer-Hansen G, Blasi F, Sloane BF, eds. *The Cancer Degradome: Proteases and Cancer Biology*. Springer; 2008:787-810.
32. Rosenberg GA. Matrix metalloproteinases in neuroinflammation. *Glia*. 2002;39:279-291.
33. Rosenberg GA. Matrix metalloproteinases and their multiple roles in neurodegenerative diseases. *Lancet Neurol*. 2009;8:205-216.
34. Rempe RG, Hartz AMS, Bauer B. Matrix metalloproteinases in the brain and blood-brain barrier: versatile breakers and makers. *J Cereb Blood Flow Metab*. 2016;36:1481-1507.
35. Wu YJ, Neoh CA, Tsao CY, Su JH, Li HH. Sinulariolide suppresses human hepatocellular carcinoma cell migration and invasion by inhibiting matrix metalloproteinase-2/-9 through MAPKs and PI3K/Akt signaling pathways. *Int J Mol Sci*. 2015;16:16469-16482.
36. Dutra FF, Bozza MT. Heme on innate immunity and inflammation. *Front Pharmacol*. 2014;5(115):1-20.
37. Cho A, Graves J, Reidy MA. Mitogen-activated protein kinases mediate matrix metalloproteinase-9 expression in vascular smooth muscle cells. *Arterioscler Thromb Vasc Biol*. 2000;20:2527-2532.
38. Wang T, Liao Y, Sun Q, et al. Upregulation of matrix metalloproteinase-9 in primary cultured rat astrocytes induced by 2-chloroethanol via MAPK signal pathways. *Front Cell Neurosci*. 2017;11(218):1-10.
39. Ryu JK, McLarnon JG. A leaky blood-brain barrier, fibrinogen infiltration and microglial reactivity in inflamed Alzheimer's disease brain. *J Cell Mol Med*. 2009;13:2911-2925.
40. Szmitko PE, Wang C-H, Weisel RD, de Almeida JR, Anderson TJ, Verma S. New markers of inflammation and endothelial cell activation: Part I. *Circulation*. 2003;108:1917-1923.
41. Bowman GL, Kaye JA, Moore M, Waichunas D, Carlson NE, Quinn JF. Blood-brain barrier impairment in Alzheimer disease: stability and functional significance. *Neurology*. 2007;68:1809-1814.
42. Menezes MJ, McClenahan FK, Leiton CV, Aranmolate A, Shan X, Colognato H. The extracellular matrix protein laminin α2 regulates the maturation and function of the blood–brain barrier. *J Neurosci*. 2014;34:15260-15280.
43. Sixt M, Engelhardt B, Pausch F, Hallmann R, Wendler O, Sorokin LM. Endothelial cell laminin isoforms, laminins 8 and 10, play decisive roles in T cell recruitment across the blood-brain barrier in experimental autoimmune encephalomyelitis. *J Cell Biol*. 2001;153:933-946.
44. Daneman R, Zhou LU, Agalliu D, Cahoy JD, Kaushal A, Barres BA. The mouse blood-brain barrier transcriptome: a new resource for understanding the development and function of brain endothelial cells. *PLoS One*. 2010;5(10):e13741.
45. Armulik A, Genové G, Mäe M, et al. Pericytes regulate the blood-brain barrier. *Nature*. 2010;468:557-561.
46. Stark K, Eckart A, Haidari S, et al. Capillary and arteriolar pericytes attract innate leukocytes exiting through venules and "instruct" them with pattern-recognition and motility programs. *Nat Immunol*. 2013;14:41-51.
47. Rudziak P, Ellis CG, Kowalewska PM. Role and molecular mechanisms of pericytes in regulation of leukocyte diapedesis in inflamed tissues. *Mediators Inflamm*. 2019;2019:1-9.
48. Asahi M, Wang X, Mori T, et al. Effects of matrix metalloproteinase-9 gene knock-out on the proteolysis of blood-brain barrier and white matter components after cerebral ischemia. *J Neurosci*. 2001;21:7724-7732.
49. Caputo T, Gilardi F, Desvergne B. From chronic overnutrition to metaflammation and insulin resistance: adipose tissue and liver contributions. *FEBS Lett*. 2017;591:3061-3088.

50. Bugno M, Witek B, Bereta J, Bereta M, Edwards DR, Kordula T. Reprogramming of TIMP-1 and TIMP-3 expression profiles in brain microvascular endothelial cells and astrocytes in response to proinflammatory cytokines. *FEBS Lett*. 1999;448:9-14.
51. Suryadevara R, Holter S, Borgmann K, et al. Regulation of tissue inhibitor of metalloproteinase-1 by astrocytes: links to HIV-1 dementia. *Glia*. 2003;44:47-56.
52. Pagenstecher A, Stalder AK, Kincaid CL, Shapiro SD, Campbell IL. Differential expression of matrix metalloproteinase and tissue inhibitor of matrix metalloproteinase genes in the mouse central nervous system in normal and inflammatory states. *Am J Pathol*. 1998;152:729-741.
53. Szymocha R, Akaoka H, Brisson C, et al. Astrocytic alterations induced by HTLV type 1-infected T lymphocytes: a role for Tax-1 and tumor necrosis factor α. *AIDS Res Hum Retroviruses*. 2000;16:1723-1729.
54. Gardner J, Ghorpade A. Tissue inhibitor of metalloproteinase (TIMP)-1: the TIMPed balance of matrix metalloproteinases in the central nervous system. *J Neurosci Res*. 2003;74:801-806.
55. Ghorpade A, Persidskaia R, Suryadevara R, et al. Mononuclear phagocyte differentiation, activation, and viral infection regulate matrix metalloproteinase expression: implications for human immunodeficiency virus type 1-associated dementia. *J Virol*. 2001;75:6572-6583.
56. Lewandowski KC, Banach E, Bieńkiewicz M, Lewiński A. Matrix metalloproteinases in type 2 diabetes and non-diabetic controls: effects of short-term and chronic hyperglycaemia. *Arch Med Sci*. 2011;7:294-303.
57. Hickey WF, Hsu BL, Kimura H. T-lymphocyte entry into the central nervous system. *J Neurosci Res*. 1991;28:254-260.
58. Ousman SS, Kubes P. Immune surveillance in the central nervous system. *Nat Neurosci*. 2012;15:1096-1101.
59. Lee CH, Shin SH, Kang GM, et al. Cellular source of hypothalamic macrophage accumulation in diet-induced obesity. *J Neuroinflammation*. 2019;16(221):1-10.
60. Profaci CP, Munji RN, Pulido RS, Daneman R. The blood–brain barrier in health and disease: important unanswered questions. *J Exp Med*. 2020;217(4):e20190062.
61. Stoll G, Jander S, Schroeter M. Detrimental and beneficial effects of injury-induced inflammation and cytokine expression in the nervous system. *Adv Exp Med Biol*. 2002;513:87-113.
62. Takeshita Y, Ransohoff RM. Inflammatory cell trafficking across the blood-brain barrier: chemokine regulation and in vitro models. *Immunol Rev*. 2012;248:228-239.
63. Cross AH, O'Mara T, Raine CS. Chronologic localization of myelin-reactive cells in the lesions of relapsing EAE: implications for the study of multiple sclerosis. *Neurology*. 1993;43:1028-1033.
64. Engelhardt B, Vestweber D, Hallmann R, Schulz M. E- and P-selectin are not involved in the recruitment of inflammatory cells across the blood-brain barrier in experimental autoimmune encephalomyelitis. *Blood*. 1997;90:4459-4472.
65. Rosenberg GA, Estrada EY, Dencoff JE. Matrix metalloproteinases and TIMPs are associated with blood-brain barrier opening after reperfusion in rat brain. *Stroke*. 1998;29:2189-2195.
66. Rezai-Zadeh K, Gate D, Town T. CNS infiltration of peripheral immune cells: D-day for neurodegenerative disease? *J Neuroimmune Pharmacol*. 2009; 4(4):462-475.
67. Luchsinger JA, Reitz C, Patel B, Tang MX, Manly JJ, Mayeux R. Relation of diabetes to mild cognitive impairment. *Arch Neurol*. 2007;64:570-575.
68. Arvanitakis Z, Wilson RS, Bienias JL, Evans DA, Bennett DA. Diabetes mellitus and risk of Alzheimer disease and decline in cognitive function. *Arch Neurol*. 2004;61:661-666.
69. Takechi R, Lam V, Brook E, et al. Blood-brain barrier dysfunction precedes cognitive decline and neurodegeneration in diabetic insulin resistant mouse model: an implication for causal link. *Front Aging Neurosci*. 2017;9(399):1-12.
70. Carvalho C, Machado N, Mota PC, et al. Type 2 diabetic and Alzheimer's disease mice present similar behavioral, cognitive, and vascular anomalies. *J Alzheimer's Dis*. 2013;35:623-635.
71. Carvalho C, Cardoso S, Correia SC, et al. Metabolic alterations induced by sucrose intake and Alzheimer's disease promote similar brain mitochondrial abnormalities. *Diabetes*. 2012;61:1234-1242.
72. Ho L, Qin W, Pompl PN, et al. Diet-induced insulin resistance promotes amyloidosis in a transgenic mouse model of Alzheimer's disease. *FASEB J*. 2004;18:902-904.
73. Yamagishi SI, Maeda S, Matsui T, Ueda S, Fukami K, Okuda S. Role of advanced glycation end products (AGEs) and oxidative stress in vascular complications in diabetes. *Biochim Biophys Acta—Gen Subj*. 2012;1820:663-671.
74. Dias IHK, Griffiths HR. Oxidative stress in diabetes—circulating advanced glycation end products, lipid oxidation and vascular disease. *Ann Clin Biochem*. 2014;51:125-127.
75. Rudich A, Kanety H, Bashan N. Adipose stress-sensing kinases: linking obesity to malfunction. *Trends Endocrinol Metab*. 2007;18:291-299.
76. Monteiro R, Azevedo I. Chronic inflammation in obesity and the metabolic syndrome. *Mediators Inflamm*. 2010;2010:1-10.
77. Spielman LJ, Little JP, Klegeris A. Inflammation and insulin/IGF-1 resistance as the possible link between obesity and neurodegeneration. *J Neuroimmunol*. 2014;273:8-21.
78. Ramage FJ, Clewlow AS, Williams LM, Macleod MR, Langston RF. Effects of dietary fat manipulation on cognition in mice and rats: protocol for a systematic review and meta-analysis. *BMJ Open Sci*. 2020;4:e100108.
79. Song SH, Hardisty CA. Early onset type 2 diabetes mellitus: a harbinger for complications in later years-clinical observation from a secondary care cohort. *QJM*. 2009;102(11):799-806.
80. Fredman G, Kamaly N, Spolitu S, et al. Targeted nanoparticles containing the proresolving peptide Ac2-26 protect against advanced atherosclerosis in hypercholesterolemic mice. *Sci Transl Med*. 2015;7(275):1-19.
81. De Coupade C, Solito E, Levine JD. Dexamethasone enhances interaction of endogenous Annexin 1 with L-selectin and triggers shedding of L-selectin in the monocytic cell line U-937. *Br J Pharmacol*. 2003;140:133-145.
82. Solito E, Romero IA, Marullo S, Russo-Marie F, Weksler BB. Annexin 1 binds to U937 monocytic cells and inhibits their adhesion to microvascular endothelium: involvement of the α4β1 integrin. *J Immunol*. 2000;165:1573-1581.
83. McArthur S, Cristante E, Paterno M, et al. Annexin A1: a central player in the anti-inflammatory and neuroprotective role of microglia. *J Immunol*. 2010;185:6317-6328.
84. Elhayany A, Lustman A, Abel R, Attal-Singer J, Vinker S. A low carbohydrate Mediterranean diet improves cardiovascular risk factors and diabetes control among overweight patients with type 2 diabetes mellitus: a 1-year prospective randomized intervention study. *Diabetes Obes Metab*. 2010;12:204-209.

85. Shai I, Schwarzfuchs D, Henkin Y, et al. Weight loss with a low-carbohydrate, Mediterranean, or low-fat diet. *N Engl J Med*. 2008;359:229-241.
86. de Lorgeril M, Renaud S, Salen P, et al. Mediterranean alpha-linolenic acid-rich diet in secondary prevention of coronary heart disease. *Lancet*. 1994;343:1454-1459.
87. De Lorgeril M, Salen P, Martin JL, Monjaud I, Delaye J, Mamelle N. Mediterranean diet, traditional risk factors, and the rate of cardiovascular complications after myocardial infarction: final report of the Lyon Diet Heart Study. *Circulation*. 1999;99:779-785.
88. Gæde P, Vedel P, Larsen N, Jensen GVH, Parving HH, Pedersen O. Multifactorial intervention and cardiovascular disease in patients with type 2 diabetes. *N Engl J Med*. 2003;348:383-393.
89. Van Den Brink AC, Brouwer-Brolsma EM, Berendsen AAM, Van De Rest O. The Mediterranean, dietary approaches to stop hypertension (DASH), and Mediterranean-DASH intervention for neurodegenerative delay (MIND) diets are associated with less cognitive decline and a lower risk of Alzheimer's disease—a review. *Adv Nutr*. 2019;10:1040-1065.
90. Wei S, Zhao J, Bai M, Li C, Zhang L, Chen Y. Comparison of glycemic improvement between intermittent calorie restriction and continuous calorie restriction in diabetic mice. *Nutr Metab*. 2019;16(60):1-11.
91. Wei S, Han R, Zhao J, et al. Intermittent administration of a fasting-mimicking diet intervenes in diabetes progression, restores β cells and reconstructs gut microbiota in mice. *Nutr Metab*. 2018;15(80):1-12.
92. Rosa CVDD, Campos JMD, Sá Nakanishi ABD, et al. Food restriction promotes damage reduction in rat models of type 2 diabetes mellitus. *PLoS One*. 2018;13:e0199479.
93. Zhang Q, Xu L, Xia J, Wang D, Qian M, Ding S. Treatment of diabetic mice with a combination of ketogenic diet and aerobic exercise via modulations of PPARs gene programs. *PPAR Res*. 2018;2018:1-13.
94. Winters WD, Huo YS, Yao DL. Inhibition of the progression of type 2 diabetes in the C57BL/6J mouse model by an anti-diabetes herbal formula. *Phyther Res*. 2003;17:591-598.
95. Hofmann SM, Dong HJ, Li Z, et al. Improved insulin sensitivity is associated with restricted intake of dietary glycoxidation products in the db/db mouse. *Diabetes*. 2002;51:2082-2089.
96. Jurado-Ruiz E, Álvarez-Amor L, Varela LM, et al. Extra virgin olive oil diet intervention improves insulin resistance and islet performance in diet-induced diabetes in mice. *Sci Rep*. 2019;9(11311):1-13.
97. McGrattan AM, McGuinness B, McKinley MC, et al. Diet and inflammation in cognitive ageing and Alzheimer's disease. *Curr Nutr Rep*. 2019;8:53-65.
98. Gómez-Pinilla F. Brain foods: the effects of nutrients on brain function. *Nat Rev Neurosci*. 2008;9:568-578.
99. Wu A, Ying Z, Gomez-Pinilla F. Dietary curcumin counteracts the outcome of traumatic brain injury on oxidative stress, synaptic plasticity, and cognition. *Exp Neurol*. 2006;197:309-317.
100. Wu A, Ying Z, Gomez-Pinilla F. Oxidative stress modulates Sir2α in rat hippocampus and cerebral cortex. *Eur J Neurosci*. 2006;23:2573-2580.

SUPPORTING INFORMATION

Additional supporting information may be found in the online version of the article at the publisher's website.

How to cite this article: Sheikh MH, Errede M, d'Amati A, et al. Impact of metabolic disorders on the structural, functional, and immunological integrity of the blood-brain barrier: Therapeutic avenues. *FASEB J*. 2022;36:e22107. doi:10.1096/fj.202101297R